Small-scale mechanical testing of materials

B. Nagamani Jaya[1] and Md Zafir Alam[1,2]

[1]Department of Materials Engineering, Indian Institute of Science, Bangalore 560 012, India
[2]Defence Metallurgical Research Laboratory, Hyderabad 500 058, India

Small-scale mechanical testing of materials has gained prominence in the last decade or so due to the continuous miniaturization of components and devices in everyday application. This review describes the various micro-fabrication processes associated with the preparation of miniaturized specimens, geometries of test specimens and the small scale testing techniques used to determine the mechanical behaviour of materials at the length scales of a few hundred micrometers and below. This is followed by illustrative examples in a selected class of materials. The choice of the case studies is based on the relevance of the materials used in today's world: evaluation of mechanical properties of thermal barrier coatings (TBCs), applied for enhanced high temperature protection of advanced gas turbine engine components, is essential since its failure by fracture leads to the collapse of the engine system. Si-based substrates, though brittle, are indispensable for MEMS/NEMS applications. Biological specimens, whose response to mechanical loads is important to ascertain their role in diseases and to mimic their structure for attaining high fracture toughness and impact resistance. An insight into the mechanisms behind the observed size effects in metallic systems can be exploited to achieve excellent strength at the nano-scale. A future outlook of where all this is heading is also presented.

Keywords: Electropolishing, materials, micro-fabrication technique.

Introduction

IN the recent years, mechanical characterization of materials at small length scales has gained significant prominence and become an intense area for research. The impetus is the need to measure the mechanical properties of materials in small volumes for several engineering as well as biological/biomimetic applications such as miniaturized electronic devices and sensors used in micro-/nano-electro mechanical systems (MEMS/NEMS), thermal barrier coating (TBC) systems for aerospace applications and biological cells, to name a few. In each of these devices/systems, the geometries are usually complex and intricate and the dimensions constrained. Further, the

constituting materials are mostly used in small volumes as thin films, the thicknesses of which usually range from a few nano-meters to about a few hundred microns. In many cases, such as that of nano-sensors, the length scale at which the materials are used remain comparable to the microstructural length scales. The material performance, and hence, the reliability of components and devices at small length scales (below a few hundred microns) remains dependent on both microstructure and size.

It is well-known that the mechanical response of materials varies with the length scale. Historically, the first account of size effect in materials was given by Leonardo who observed lower fracture strengths in shorter wires[1]. Several centuries later, Griffith reported an increase in fracture stress in glass fibres with reduction in the fibre diameter[2], while Hall and Petch discovered increase in yield strength of metallic materials with reduction in grain size[3,4]. Subsequently, a number of studies were carried out to find the effect of flaws and their statistical distribution on the likelihood of failure of metallic whiskers[5–7]. The findings from the above studies, that several material properties such as yield strength, ductility and fracture toughness increase with reducing length scales in all classes of materials, seemed to give credence to the popular belief that 'smaller is stronger'.

However, in recent times, there have been reports of reversal of observed trends in mechanical behaviour of materials at even smaller length scales, such as that at a few nano-metric levels[8,9]. Such reports, while they remain debatable, have generated a lot of controversy and confusion surrounding material properties at small length scales[10]. One of the reasons cited for the reversal in mechanical response of materials at the lowest length scales is the overlap between the length scale of defects controlling the deformation of materials with that of the specimen dimensions, leading to a breakdown in the assumptions of continuum mechanics[1]. For instance, with increasing refinement, the ratio of surface area to volume increases dramatically at nano-metric length scales. During deformation within such small volumes of material, the nature of interaction between the inherent defects and that generated during deformation changes, because the defects tend to escape from the surface. Therefore, due to the changing nature of interaction between the inherent defects and that generated during deformation, conventional defect hardening theories fail to account for the strength in such materials. A classic example is the reverse Hall–

Petch effect wherein the strength of a material decreases with refinement in grain size below about 40 nm (ref. 8). Therefore, mechanical properties of materials evaluated in small volumes differ significantly from those evaluated in bulk form due to both geometric and microstructural constraints[9].

As mentioned in the preceding paragraphs, the materials in miniaturized devices are used in the form of thin films, the thicknesses of which often remain comparable to the microstructural length scale. Processing of thin film materials usually involves vapour phase deposition or electro-deposition techniques[11]. The inherent microstructure, composition and the attendant defect structure in these films are known to be affected by the processing method adopted. Under such circumstances, where the dimensional length scale of the material remains comparable to the microstructural length scale and the composition as well as the defect structure varies within the material, it becomes essential to evaluate the mechanical response of materials at length scales that are similar to that used in actual application. The properties, thus evaluated, will be representative of the thin film and can be used in models for assessing the reliability and durability of miniaturized devices. Further, such studies on the evaluation of mechanical behaviour of thin films are important from the point of scientific understanding of deformation mechanism of materials in small volumes.

Choice of the small-scale testing technique is made depending on the structure of interest (i.e. whether the film is free standing or constrained, thin, thick or an interface), the stresses that the final device experiences, the mechanical properties to be determined and the characteristics of the test structure itself like ease of fabrication, assembly and testing[12]. Considering the above aspects, mechanical testing of small structures has diversified over the last decade and today includes tensile tests, bending/curvature, pillar compression, depth sensing indentation, atomic force microscopy (AFM) based cantilever methods and micro-electromechanical system approaches. A variety of advanced micro-fabrication methods such as focused ion beam (FIB) machining, computerized numerically controlled (CNC) machining, electro discharge machining (EDM), laser-based processes, lithography, lithographie galvanoformung abformung (LIGA) and electro-deposition have been adopted for fabrication of specimens at the micro-meter and sub-micro-meter length scales[13,14]. Prior to testing, the specimen is accurately positioned and aligned with respect to the loading axis. During testing, the mechanical response of the material is obtained from the variation in the load-displacement characteristics which is recorded using a high resolution load cell and displacement sensors as well as *in-situ* imaging of specimen deformation[15,16].

However, though several methods for small scale testing of materials have evolved, there are no standards available with respect to the design of miniaturized test specimens. Further, as the nature of stresses and strains within the specimens varies with the specimen geometry and the loading configuration adopted during the test, the lack of analytical solutions compels the use of modelling-based techniques to find approximate solutions for stress and strain fields. A good agreement between simulation and experimental results becomes essential especially due to the lack of well-established standards in this field. Therefore, concurrent with experimental methods, a number of simulation techniques such as finite element modelling, strain gradient plasticity, discrete dislocation dynamics, molecular dynamics, Monte Carlo methods and density functional theory have been developed to model material properties at different length scales. Each of them is valid only in a particular size range, depending on the underlying assumption on which it is based and computational power required to model that size scale.

There are already many reviews available on small scale testing in the literature[12,17–23]. While some of them concentrate on the testing technique and instrumentation issues, others describe the size effects that become significant as we go to lower size scales. Prorok[21] has comprehensively reviewed issues in micro- and nano-mechanics, covering instrumentation and material properties as well as theories and models explaining the same. In this review, we will first give an account of the various fabrication and testing techniques used in small scale systems, with a brief regarding each of their advantages and limitations. This will be followed by a description of mechanical properties of a select set of materials evaluated at small length scales. The material components have been chosen to demonstrate the indispensability of small scale testing in extracting particular properties from different classes of materials. The material systems chosen for illustration in the present review are TBCs, Si-based MEMS and biological systems including cells and nacre-shells. Attempt has been made to present an overview on size effects vis-à-vis structural properties of metallic materials such as Cu, Al, Ag, Ni, Fe, Mo, Nb and W, as evaluated using various small scale testing techniques. The choice of the above metals naturally follows as they form the principal constituents of most small-scale structures and devices. The mechanical properties determined by small-scale testing of the above materials and the micro-mechanisms associated with their deformation, as reported by various groups are discussed.

Micro-fabrication techniques

Specimen preparation methods for small scale testing depend on the type of test to be carried out and the size of the component being tested. Controlled architectures may be fabricated with nano-scale precision today. Nano-indentation only requires a smooth, polished specimen

surface while an *in-situ* tensile tester within an optical/electron microscope requires elaborate and accurate micro-machining of both the grips and the sample. The different techniques for micro-machining have different precisions and remove material by distinct processes such as mechanical force, melting and evaporation, ablation, plastic deformation, dissolution, solidification, lamination or re-composition[13]. The methods used for micro-fabrication and the parameters controlling them can influence the mechanical properties of the resulting material system as they affect the grain size, structure and texture of the resulting specimen. In a few other cases, artificial damage will be induced in the specimen due to ion implantation, deposition of unknown impurities or formation of a heat-affected zone. Broadly, fabrication methods can be classified into two types depending on whether they follow a top-down or bottom-up approach. While photolithographic and LIGA techniques involve building the system layer by layer using a mould, micro-EDM, laser cutting, reactive ion etching, electro-polishing and FIB involve machining or removing material from the bulk system to the required shape[22]. Masuzawa[13] has given illustrative examples of features that can be machined using some of the more popular micro-machining processes such as EDM, LIGA, micro-punching, laser-based cutting and 3D micro-milling. Some of these methods of specimen fabrication are described below:

Micro-EDM and laser-based CNC machining[13]: EDM uses an electrostatic discharge between the electrode and work-piece to remove material. A dielectric fluid is used to flush away debris and act as coolant in the erosive technique. Custom made shapes can be machined out using micro-EDM but only electrically conducting samples can be cut by this process. Also, the minimum sample dimension that can be machined is limited by the sum total of the wire diameter and the heat-affected zone, which as of today stands at 30 μm. Laser-based cutting processes use a high power Nd–YAG or CO_2 focused laser spot, controlled by using a computer, remove material parts by burning/etching/evaporation. Control is achieved by modifying parameters such as laser power, cutting speed and number of passes. A jet of gas can be used to blow away material. A positioning accuracy of 10 μm and tolerance up to 25 μm can be achieved in modern laser cutters. Both the EDM and laser-based processes are integrated into a computer-aided designing/modelling (CAD/CAM) program for precise control.

Focused ion beam machining[22]: FIB uses a liquid metal (typically Ga) ion source. On applying a large enough voltage in an evacuated chamber, the metal ionizes and bombards the surface of the specimen to sputter away material. FIB is a versatile tool, with the ability to micro-machine metallic and semi-conducting as well as insulating materials to an extent, while providing for tolerances

in the nano-meter range. Today's dual beam FIB systems are capable of micro-milling, gas-assisted etching, deposition and cross-sectioning and serial sectioning. There are some drawbacks as well. The process is time consuming and hence expensive for machining at a large scale. Sputtering brings about ion implantation damage which can alter the properties of the material, especially in the sub-surface damage-affected zone.

Deep reactive ion etching (DRIE)[24]: This process uses a chemically reactive plasma to remove material deposited on wafers. A strong radio frequency (RF) field is applied in vacuum to initiate the plasma and a gas is purged in as the etchant. RIE can achieve limited etch depths of ~10 μm at a rate of 1 μm/min and is mainly used in IC manufacturing. In DRIE, deeper penetration and higher aspect ratios of up to 30 are possible using highly anisotropic etchants and this procedure has been mainly developed for MEMS technology.

Lithography[22]: It basically involves several steps: deposition of a sacrificial layer on the Si substrate, patterning it to the required shape using selective masking, depositing the desired material (metal/ceramic/polymer) by sputtering or physical vapour deposition (PVD) and chemical vapour deposition (CVD) processes and etching away the underlying substrate and sacrificial layers to produce free standing structures of the deposited material. The procedure is most commonly used to fabricate Si-based MEMS systems. Small aspect ratio of the product limits its use to mainly the semi-conductor industry. Several variants to lithographic techniques have been developed for fabrication of different classes of materials. These can be classified into three basic categories: bulk micro-machining, surface micro-machining and LIGA. Photolithography is based on a projection-printing system used for projection of an image from a mask to a thin-film polymer based photo-resist, which is itself sensitive to UV light but resistant to chemical attack. The photo-mask comprises a glass plate with the desired metal pattern and is transparent to UV light. The resolution of photolithographic techniques is limited by optical diffraction limits. Soft lithography is used for biological materials and uses an elastomeric stamp or mould to generate micro-patterns either by contact printing, embossing or replica moulding. The poly-dimethyl-siloxane (PDMS) based stamps themselves are generated by photolithographically patterned masters. E-beam lithography is a fairly new addition to this family where the electron beam is used to pattern materials on resists. It is mainly used in IC chips and development of nanotechnology architectures as it provides for nano-metric precision and resolution in machining.

LIGA[22]: It is a combination of lithography, electroforming and plastic moulding. It uses a combination of X-ray

or UV lithography and electroplating procedures to mould the components to the required shape. Polymer moulds are made from X-ray lithography following which the metal is deposited by electroplating. The master mould can be replicated in mass production. Though more popularly used with metal-based MEMS systems, a variety of non-Si materials can be processed with this technique. The MEMS devices produced from LIGA have higher aspect ratios and are sturdier. LIGA is a batch process useful for mass production.

Electrochemical micromachining and electropolishing[14]: This process involves the reproduction of the cathode shape on the anode by high rate anodic dissolution. But like other micro-machining processes, a photosensitive polymer is first coated on the metal part and irradiated through a suitable mask to produce the desired pattern, following which the positive and negative photoresist are chemically dissolved and the exposed metal is subjected to electrochemical dissolution, forming the final shape. The process is faster than chemical routes, eliminates the use of oxidizing agents and can machine chemically resistant metals and alloys with ease. This process can produce scale resolved surface structures in the micro-meter and nano-meter scales.

Patterned SAMs (self-assembled monolayers)[25]: SAMs of organic molecules consist of a head group, tail group and functional group and form spontaneously as molecular assemblies by chemi-sorption of the head group on a substrate from a vapour or liquid phase. They then organize themselves into monolayers, forming large ordered domains. Thiols on gold or other noble metal substrates are the most commonly used SAMs, which can be extended to NEMS and amenable to nanolithography. The metal substrate itself can be produced by PVD or electrochemical routes. SAMs can be patterned using various techniques: micro-contact printing, dip-pen nanolithography, UV irradiation or by shaving by AFM/STM tips. The tail group can be modified to attract and attach to a specific nanoparticle.

Testing – instrumentation, advantages and limitations

Testing at the small scale poses many challenges with respect to positioning and handling of the specimen as well as with accurate application of force and reliable measurement of load/displacement during deformation. The choice is generally between the ease of fabrication, instrumentation and testing vis-à-vis the ease of data interpretation, analysis and parameter extraction[12]. The test structure itself can be integrated or not integrated to the active mechanical device. Some of the methods deal with free-standing films and others handle the coating-

substrate combination as a whole. The boundary conditions, planarity of the test structure and the dimensional characteristics of the specimen become increasingly important as one goes into smaller domains of testing. There are a variety of actuators that can be used for deforming the specimen-thermal, electrostatic, piezo-electric, shape memory effect and magnetic. They are attached to a transducer to convert electrical energy to mechanical work. Capacitance probes with a resolution of 10 nm are available for measurement of the motion of the movable grip[15]. Commercial load cells today possess a load resolution of 0.001 g, while commercial nano-indenters exhibit resolutions of up to 1 nN and sub-nanometric displacement resolution as well[22]. As these instruments are sensitive to noise, vibration isolation becomes an important part of small scale testing. Most of these methods also require non-contact strain measurement techniques as contact-based methods have a high chance of adding to errors during the course of the measurement at such miniaturized scales and also damaging fragile specimens. Laser extensometry, interferometic strain displacement gauge (ISDG) and digital image correlation (DIC) make use of natural/artificial markers to track displacements. *In-situ* testing methods inside the scanning electron microscope (SEM), transmission electron microscope (TEM) and AFM have become popular of late due to the direct viewing of deformation process made possible during the test. The testing methods described here are by no means exhaustive, with new geometries and instruments being developed every day. A few of the test geometries used at the small scale are shown in Figure 1.

Micro-tensile testing: In micro-tensile testing, the mechanical behaviour of a material is determined under uniaxial loading using a miniaturized specimen[20,23]. The strain generated in the specimen during uniaxial loading remains uniform over its thickness. Therefore, the results obtained from micro-tensile testing are easy to interpret. This method has been adopted for evaluating the properties of free-standing coatings, including those with graded composition and microstructure, such as bond coats.
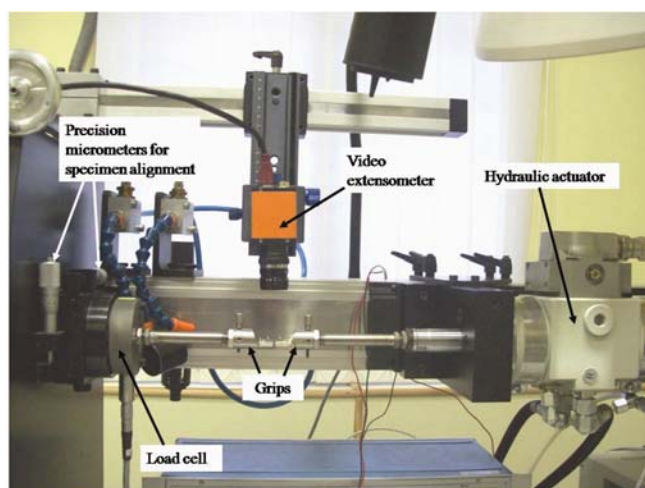
A typical micro-tensile testing machine incorporates all the basic features of a conventional macro-tensile testing machine. It consists of a load train, a hydraulic actuator for straining the sample and a data recording system (Figure 2). However, the instrumentation involved in a micro-tensile test machine is significantly more sophisticated than in its macro-counterpart. The resolution in commercial micro-tensile testing machines is capable of accurately measuring a load as low as 1 mN. The alignment of the specimen with the loading axis is achieved by the use of a precision micro-manipulator, micro-meters and magnifying lenses[20,23,26,27]. As the small size of the specimens precludes the possibility of placing the
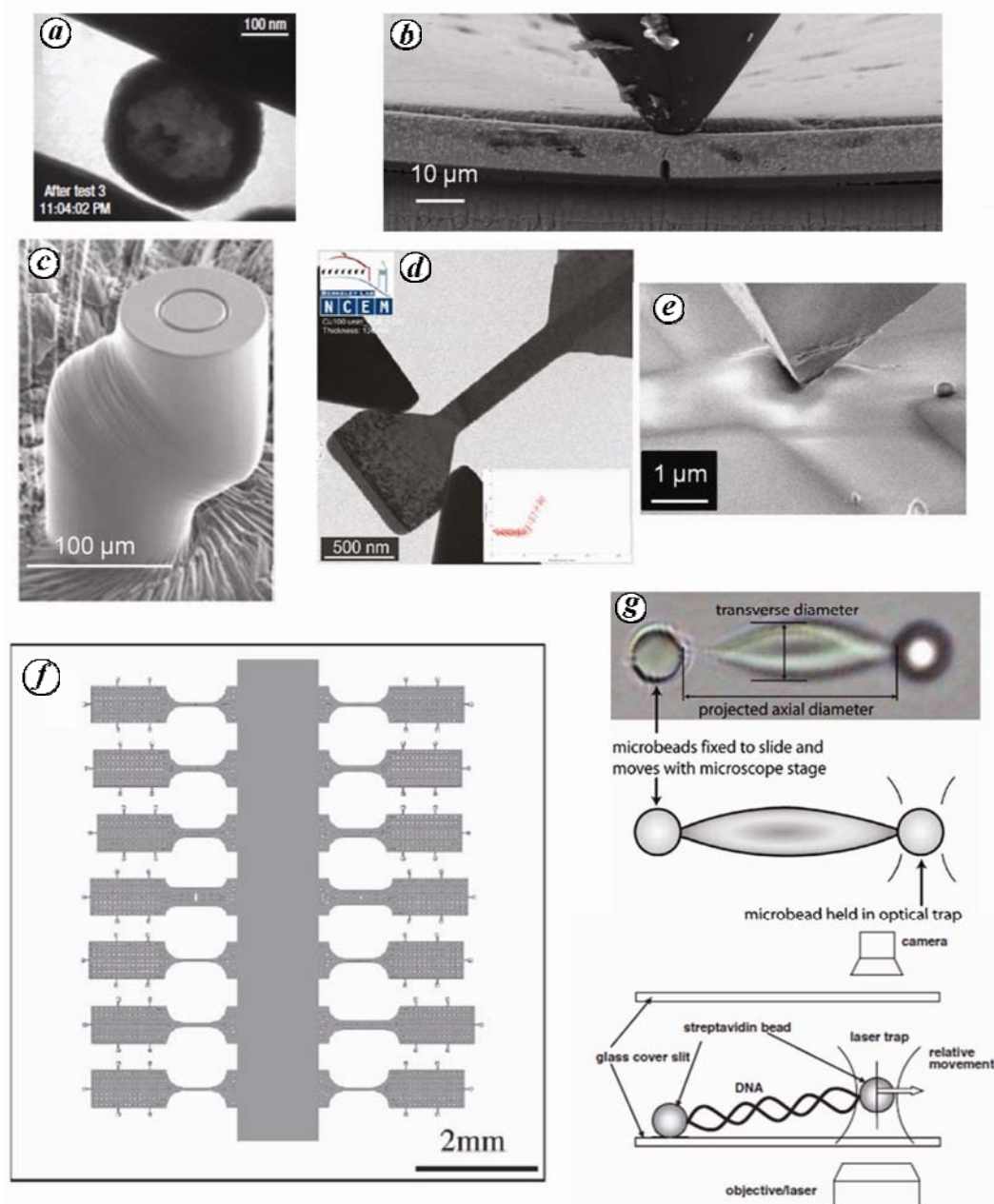
Figure 1. Commonly used small-scale testing geometries: *a*, *In-situ* TEM compression of nanospheres[167]; *b*, *In-situ* SEM microbeam bending[182]; *c*, Micro-pillar compression[183]; *d*, *In-situ* TEM tension with special grips[165]; *e*, *In-situ* SEM based indentation[184]; *f*, MEMS-based tension[185]; *g*, Optical tweezers for testing biological specimen[132].

extensometers in direct physical contact with the specimen, the strain in the specimen is measured using a non-contact extensometry technique such as interferometry[20,23], high resolution capacitance gauge[28], video-extensometer[29], DIC[30,31] and differential digital image tracking (DDIT)[32]. For carrying out high temperature test, the specimen is heated to the desired temperature either in a furnace or by resistance heating (by passing DC current). The temperature measurement is carried out either by using a thermocouple placed in proximity to the sample or by using a radiation pyrometer[23,33].

Carrying out micro-tensile testing of free-standing coatings, especially the brittle ones, is challenging because of experimental and other associated difficulties. In case of testing of bulk tensile specimens, sample dimensions and test procedures are well established in the form of accepted standards[34,35]. However, in case of micro-tensile testing, where the thickness of the specimen is often less than a few hundred micrometers, no such standard exists at present. In the literature, a few micro-tensile sample configurations have been reported. Samples with V-shaped ends and curved/parallel guage have

Figure 2. Micro-tensile testing machine in DMRL. Courtesy: Walter-Bai Ag, Switzerland.

been reported[20,23,36]. Other sample shapes such as rectangular stick[37,38], hour glass[36,38–40] and dog-bone with rectangular paddle[19,40,41] have also been used for evaluating the tensile properties of thin films.

Another major issue associated with micro-tensile testing is the method to be used for gripping the sample during the test. This issue is especially important in case of brittle samples. These samples if gripped in a conventional manner between two flat platens, often tend to break at the neck or fillet region. To avoid this problem, several improvized methods have been adopted including gluing each end of the sample on a single platen[23,30] and gluing of the whole sample onto a compliant substrate[19,40]. Use of slotted grips has also been reported wherein the sample ends are held firmly during the test against the walls of the slots appropriately made in the grips[20,23,31,33]. Apart from the issue of sample gripping, fabrication of micro-tensile specimens is also a challenging task as it involves precision machining and polishing. Methods such as EDM[20,23,31], LIGA[20,23], etching[23,41–43] and DRIE[23,43] are some of the methods that have been reported for the preparation of micro-tensile samples.

Pan et al.[33] have evaluated the tensile behaviour of a free-standing low activity Pt-aluminide coating in the temperature range RT-1200°C using the micro-tensile testing technique. They have also studied the creep behaviour of the above bond coat using the same technique. Micro-tensile testing method was also adapted by Alam et al.[44] to evaluate the tensile behaviour of free-standing high activity Pt-aluminide bond coat at various temperatures and strain rates ranging from RT-1100°C and 10^{-5}–10^{-1} s^{-1}, respectively. In a recent study, the micro-tensile test method has also been used for the evaluation of elastic behaviour of a TBC system[45].

Advanced indentation-based techniques: (Conventional indentation, micro/nano pillar compression): The depth

sensing indentation instrument has diverse applications in small scale testing. Apart from conventional nano-indentation experiments for modulus and hardness measurements, customized indenter tips can be used for pillar compression and cantilever bending from which properties like yield, fracture stress and fracture toughness can be extracted.

Nano-indentation tests are preferred due to the minimal sample preparation required and the ease of testing, though the results are difficult to interpret due to the complex state of stress experienced underneath an indenter. A diamond tip of well-defined geometry is brought into contact with the polished specimen surface and both the load (P) and displacement of the indenter (h) within the material recorded during the loading and unloading phases of indentation, from which various material properties are later determined. The features of the P–h curve provide signatures for onset of plasticity, fracture, phase transformation and hardening[46]. They can be carried out on all classes of materials and are especially useful for probing residual stress, fracture properties, adhesion, friction, time dependent deformation and modulus mapping in nano-crystalline materials, composites, soft biological specimen, amorphous materials in different structural states, thin films, multilayers and microelectronic devices[47]. High-temperature testing and *in-situ* imaging inside SEM or TEM are recent accessories that have been developed in combination with indentation by companies like Hysitron, Nanomechanics and Agilent Technologies to name a few. Sharp indenters used in nano-indentation, like the Vickers, Berkovich or cube geometries, impose a complex 3-dimensional stress field and accompanying strain gradients beneath the indenter due to which the ease of testing gets overwhelmed by the complications in the analysis of data. Errors can creep in due to many reasons, like substrate effects in thin films, gradients and heterogeneities in microstructure and pile-up in soft and strain hardening materials for which different correction factors have been proposed. Indentation size effect, which is a purely geometric effect at low indentation depths, has to be overcome as well, for valid measurements to be possible[47]. Currently, instruments can provide resolutions lower than 1 μN in load and 1 nm in depth. Schuh[46] has reviewed many of the possible material properties that can be extracted via nano-indentation in combination with other characterization tools.

Flat punch indenters are routinely used to push micro/nano-pillars and spheres in compression. Such tests have been carried out *in-situ* inside the SEM or TEM, with simultaneous recording of the P–h curve to correlate the events during pillar deformation to features like the pop-ins in the curve. Single crystal and polycrystalline metallic specimens, multilayer thin films and laminates as well as brittle ceramics have been examined by pillar compression for determining the onset of plasticity or fracture, study of deformation mechanisms and size

effects in materials using different aspect ratios of pillars[48–50]. Frictional effects at the contacting surface and properties of the supporting substrate at the bottom have to be accounted for, as do errors due to taper and bending or buckling of pillars at large aspect ratios.

Bending and curvature: (i) *Micro-beam bend tests*: This method involves bending free-standing micro-cantilevers to fracture using wedge or AFM tips attached to a nano-indenter. The cantilever beams can be of different configurations; single, double, clamped and notched, and their deformation approximated using formulae from simple beam bending theory[51]. The analytical solutions are very sensitive to beam dimensions, which must be accurately measured. Such tests are routinely used to determine the reliability and elastic properties of Si-based MEMS systems as well as to find plastic properties of single crystals and bi-crystal interfaces and fracture toughness of coatings[52]. The stiffness of the support, substrate properties and contribution of the indenter stress field and positioning of the indenter itself are considered during modelling of these structures to determine the actual stress being experienced by the beam.

(ii) *Curvature measurement*: Wafer curvature measurement of the substrate before and after film deposition, using a laser source, is a routinely used method of residual stress measurement in thin films and coatings. Coatings and thin films deposited on a substrate induce a convex or concave curvature to the substrate depending on the thermal expansion coefficient difference between the two. The method makes use of the Stoney's formula of a direct correspondence between the stress in the film and the radius of curvature of the substrate to make quantitative estimates of the residual stress in the film when confined to the substrate[53]. The main drawbacks are a requirement of a thick enough substrate and the fact that surface asperities cannot be accounted for.

(iii) *Bulge testing*: Free standing thin films are clamped at the two ends and a pressure force is applied from one end to bring about tensile stresses in the membrane. The applied pressure and deflection of the membrane (bulge height) are independently measured to determine the in-plane mechanical properties of the film like yield or fracture strength while avoiding substrate effects[54].

(iv) *Miniaturized disc bend testing (MDBT)*: This testing technique, also known as 'small punch testing', is another bend test technique that has been adopted for the evaluation of mechanical behaviour of coatings[55]. The specimen used in MDBT is a disc-shaped stand-alone coating. As the specimen is devoid of the substrate, the results obtained from MDBT are representative of the coating. The sample preparation for MDBT involves extraction of disc-shaped coupons from coated superalloy strips by electro-discharge machining. Subsequently, the discs are polished from one side to remove the substrate. Polishing is carried out till the thickness of the disc becomes equal to the thickness of the coating, i.e. till the entire substrate gets removed. The disc specimen is inserted between the upper and lower die, where the inner edge of the lower die hole acts as support, as shown in Figure 3. The specimen is then held against the die by means of holding rings while loading is applied by means of a spherical indenter connected to a punch. High-temperature testing is carried out by heating the specimens in a furnace. Application of the load causes bending in the coating similar to that of a membrane. The deflection in the specimen is recorded in a computer or a suitable recording machine.

Miscellaneous techniques: (i) *MEMS based chip tests*: Electrostatic actuation using MEMS-based actuators can be used to test Si based polycrystalline or thin film specimens on-chip, while being attached to the device[30,41,56–58]. Tensile, flexure and torsional loads have been applied by this method. The actuation is provided by comb fingers or parallel plate capacitors and the method is adopted in cases where the specimen fabrication outside the device assembly is difficult without introducing contamination, especially in bulk. Also complexities of gripping and data acquisition can be avoided. This method has also been used extensively for fatigue property determination as cyclic loading at high frequencies can be carried out with MEMS-based systems[59].

(ii) *Manipulators*: Micro- or nano-manipulators attached to light or electron microscopes are particularly useful in attachment and testing of nano-wires, particles and tubes[18]. Micro-manipulators were first developed as
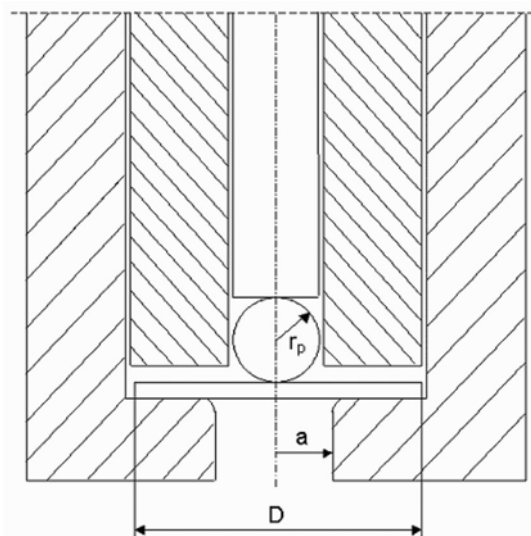
Figure 3. Schematic of the MDBT test set-up. The parameters r_p, a and D denote the radius of the ball, support radius and specimen diameter respectively[55].

extensions of scanning tunnelling microscopes (STM) and AFM[60,61], with an added advantage of real time visual feedback in ambient conditions of testing. Hatamura *et al.*[62] pioneered their use as positioning systems inside the SEM using ultrasonic motors and ball screws, providing up to 70 nm resolution. Finer movements are made possible by integrating piezoelectric slip-stick actuators and parallel plate structures[63]. Robotic control systems are used to generate appropriate driving voltages, control the gripper, plan the trajectory, process images and give closed loop feedback. Today there are various groups across the world who have built their own customized SEM-based nano-manipulators with long range movement, fine positioning (~5 nm) and flexibility up to 6 degrees of freedom[64].

(iii) *Micro-scale techniques for biological specimen testing*: AFM uses a sharp tip at the end of a flexible cantilever to measure the lateral and vertical displacement between the sample surface and tip on application of load using a piezoelectric controller[65]. The interaction of the tip with the specimen produces deflection of the cantilever, which is measured using a laser-photodiode combination at the back of the cantilever. The resolution provided by the instrument is in pico-newtons and can image atomic scale features. It is mostly used to measure elasticity and adhesion of nano-scale structures. Optical tweezers exploit the laser as a trap to manipulate particles, using the difference in refractive index of the dielectric particle with respect to the medium it is placed in, to attract the particle to the focal point of the laser[65]. This particle (e.g. glass bead) is attached to the test specimen by capillary force. Micro-pipette aspiration uses the suction pressure of the pipette to suck a single cell partially or wholly into it, and simultaneously recording the shape change as a measure of elongation[65]. All the above techniques are extensively used in the study of biological specimens in their native environments.

Illustrative examples

Evaluation of mechanical behaviour of thermal barrier coatings

TBCs are applied on Ni-base superalloy components, such as blades and vanes, operating in the hot sections of gas turbine engines for providing protection against oxidation/corrosion and heat load[66–70]. A typical TBC system is multi-layered and constituted of an inner metallic bond coat and an outer ceramic coating (Figure 4). The bond coat is about 50–100 μm in thickness and is usually an intermetallic aluminide-based coating. It serves as the source of Al required for the formation of protective Al_2O_3 scale during high temperature exposure above 1000°C, and thereby, provides oxidation resistance[66,67].

The ceramic coating, usually 150–200 μm in thickness, consists of yttria stabilized zirconia (YSZ) and provides insulation to the components against heat load. As a consequence of the application of TBCs, the overall temperature capability of the components gets enhanced significantly by about 100–150°C (refs 66–70).

During service, apart from high temperatures, turbine engine components experience complex thermo-mechanical stresses. While centrifugal mechanical stresses result from high speed rotation of the components, additional dynamic stresses are caused by varying geometries of the components and the associated variation in pressure, velocity and composition of gas flow. Significant temperature inhomogeneities over the dimensions of the components also cause generation of additional thermal stresses. Further, the components often experience sudden impact loads caused by foreign objects[66,67,70]. Besides, the components in a gas turbine engine also undergo oxidation and corrosion-induced degradation due to the reaction of the hot component surface with oxygen and/or corrosive gases present in the turbine atmosphere. The high gas flow velocity and particulate materials contained in the gas stream also causes erosion of the components. The above stringent operating conditions make the TBC prone to cracking and delamination during service.

Among the layers constituting TBC, the bond coat, in particular, is known to affect the durability of TBC, and hence, the mechanical response of the component. The bond coat is based on the intermetallic NiAl system which is an ordered phase and has a body centered cubic (b.c.c.), i.e. B2 structure. Though the NiAl phase exhibits good oxidation resistance, it is inherently brittle, and has a high brittle-to-ductile-transition-temperature (BDTT), typically above 650°C (refs 33, 44 and 55). Cracks formed in the coating during service can potentially deteriorate the overall mechanical response and strain tolerance of the coated component[70]. Further, the bond coat also undergoes dynamic changes in its composition and the attendant microstructure during high temperature exposure. Loss of Al from the coating occurs due to the formation of alumina layer on the coating surface and diffusion of Al from the coating to the substrate. At the same time, the coating gets enriched in Ni due to the outward diffusion of Ni from the substrate to the coating. As a consequence, the B2-NiAl phase starts transforming to γ'-Ni₃Al + B2-NiAl phase, the volume fraction of γ'-Ni₃Al increasing at the expense of B2-NiAl (refs 71–73). Cracks formed along the boundaries of the γ'-Ni₃Al and B2-NiAl phase are known to adversely affect the tensile behaviour of coated superalloy specimen[73]. Further, the B2-NiAl phase also undergoes a reversible martensitic transformation at temperature of about 700°C (refs 31 and 33). The stresses associated with the above phase transitions in the bond coat are known to aid in rumpling and ratcheting of the bond coat surface and cause delamination of the overlying
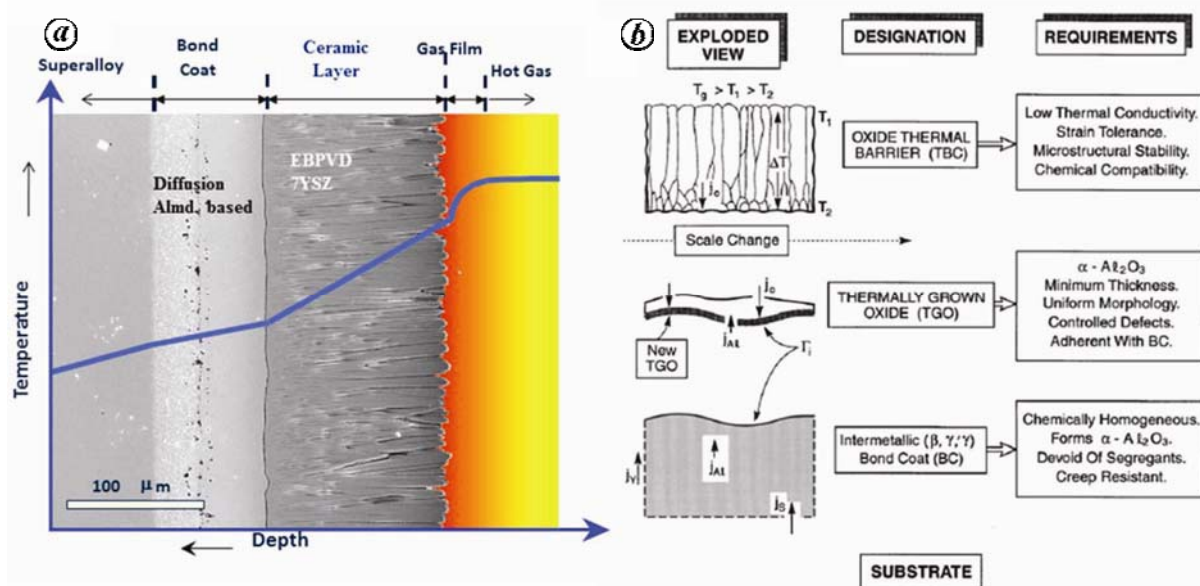
Figure 4. *a*, Exploded view of a TBC system indicating the functional requirements of each layer[70]; *b*, A typical TBC system on an aero-engine component[68].

ceramic YSZ coating. Details on the mechanisms of failure of TBCs have been reported in ref. 31.

In light of the above, understanding the mechanical behaviour of TBCs, in as-deposited condition and after thermal exposure, becomes important both from the point of views of their application in gas turbine engines as well as scientific understanding. The mechanical behaviour of bond coats has been evaluated by carrying out testing of coated bulk superalloy specimens[73–77]. Such studies mostly provide a comparative assessment of the mechanical behaviour of the coated and uncoated substrate alloy, i.e. indicate the effect of the presence of the coating on the mechanical response of the substrate alloy. However, it is difficult to ascertain the true mechanical response of the coating from these tests because of the significant differences between the coating and the substrate in terms of their section thickness and deformation characteristics. For instance, the mechanical response of diffusion aluminide (B2-NiAl) based bond coats, which are heavily graded in composition, will be significantly different from that of bulk B2-NiAl. Similarly, the mechanical behaviour of columnar YSZ ceramic coating, deposited using EB-PVD process, will be different from that bulk YSZ. Therefore, in recent times, mechanical testing of bond coats in stand-alone condition, i.e. without having any attached substrate, has been carried out for the evaluation of their mechanical behaviour. In the absence of substrate, the results of such tests provide a true representation of the bond coat. Further, the data obtained from mechanical testing of the stand-alone coating can be used in models for predicting the lifetime of TBCs, which otherwise, are based on mechanical properties of bulk B2-NiAl and YSZ phases. This aspect is

crucial as the mechanical behaviour of TBCs is affected by its inherent morphology and phase constitution. To this end, various groups have been working on the evaluation of mechanical behaviour of TBCs alone, by micro-mechanical testing technique. Some of these studies are elucidated below.

(i) *Indentation-based techniques*: Indentation method has been used for determining the hardness of TBCs at various temperatures[78]. Hardness measurements were carried out on the cross-section of an as-deposited and thermally aged TBC system at various temperatures between 25°C and 1000°C (ref. 78). Their studies indicate that the hardness of the EB-PVD YSZ coating decreased from about 3 GPa to 1 GPa with increase in temperature from 25°C to 1000°C. The diffusion Pt-aluminide (PtAl) bond coat also exhibited a decrease in hardness with increase in temperature; the decrease in hardness of the bond coat being more appreciable above about 600°C. Based on the variation in hardness with temperature, Zhang *et al.*[78] determined BDTT of the bond coat as 580 ± 30°C. The BDTT in turn was assigned as the temperature corresponding to the onset of appreciable decrease in hardness of the bond coat. They also examined the effect of thermal ageing on the hardness of TBCs. Sintering, associated with thermal ageing, caused an increase in hardness of the EB-PVD ceramic YSZ coating from about 3.5 GPa to 10 GPa. The average hardness of the bond coat after ageing (~7 GPa) was also higher than that of the as-deposited bond coat (~5 GPa), the reason for which was ascribed to the formation of martensitic B2-NiAl phase in the coating[78]. They also studied the variation in spatial hardness across the thickness of as-deposited and aged PtAl bond

coat. In the as-deposited bond coat, the hardness of the outer layer was lower at about 4 GPa whereas the hardness of the intermediate layer and that of the IDZ were higher at about 5.5 and 7 GPa, respectively. On the other hand, the hardness across the thickness of the aged bond coat remained constant in the 6–8 GPa range. Variation in hardness of various bond coats with temperature was also reported by Dryepondt et al.[79]. Their studies also revealed the decrease in hardness of the coatings with increase in temperature. Based on the variation in hardness with temperature, the BDTT of the aluminide bond coat was reported as 600°C (ref. 79). Alam et al.[80] carried out hardness and elastic modulus measurements across the thickness of a three-layer high activity PtAl bond coat at room temperature. Their study indicated that the hardness of the intermediate layer (4.81 GPa) of the coating was lower than the outer layer (8.39 GPa) and the IDZ (7.33 GPa). The variation in elastic modulus also showed a similar trend, the values being 302, 244 and 411 GPa for the outer layer, intermediate layer and IDZ respectively. The residual stress in TBCs has also been determined by indentation method. A finite element method (FEM) based analysis of the load (P)-displacement (h) characteristics has been used for this purpose[81].

Although the indentation method provides opportunity to evaluate the mechanical properties of a coating without any interference from the substrate, these properties represent extremely localized regions of the coating. Estimation of the overall mechanical properties of the coating based on such localized data may not be easy especially in the case of graded coatings such as PtAl bond coats. Further, as the stress state beneath the indenter is complex, the properties that are determined based on hardness and load-displacement curves may not be accurate because of the approximations involved in such property determination. Nevertheless, the indentation technique continues to be widely used for evaluation of mechanical properties because of the simplicity in sample preparation and ease of conducting the test.

(ii) *Bend tests*: This technique has been mostly devoted to study the crack propagation behaviour in coatings and determine their fracture toughness. Three-point and four-point bend tests have been carried out on micro-beam specimens constituted of bond coat/substrate ensemble, where the dimensions of the micro-beam specimens are usually established either by using the standard ASTM correlations existing between the various dimensional parameters or by using parametric FEM-based simulations. The test specimen is extracted from a coated strip using a combination of machining and precision polishing. A notch of desired depth is then made on the coated surface of the specimens by focused ion beam (FIB)[82]. Subsequently, load is applied in a controlled manner and the load-displacement characteristics during the test are obtained with the help of a computer or other suitable recording device. Bending in the beam, caused by the application of load, results in the generation of tensile stresses in the coating and propagation of the notch.

In a three-point bend test carried out on a diffusion aluminide bond coat micro-beam specimen, Potnis et al.[82] used the decrease in load associated with propagation of the notch and the corresponding cracking behaviour to study the variation in fracture toughness across the thickness of the bond coat. Their study revealed that the fracture toughness of the coating increases from 0.5 to 10 MPam$^{1/2}$ with increasing depth from the coating surface. In a different set of experiments at an even smaller length scale, Jaya et al.[83] and Webler et al.[84] examined the fracture behaviour of individual zones of the bond coat using micro-beam bending experiments with slightly different geometries. Webler et al.[84] adopted the micro-cantilever bending geometry for fracture toughness determination of low activity coatings, with an edge notch close to the fixed end and bent them using a nanoindenter. They reported a minimum in fracture toughness (1.4 MPa.m$^{1/2}$) for the stoichiometric, i.e. equi-atomic, NiAl and a higher fracture toughness (2.7 MPa.m$^{1/2}$) for Ni-rich NiAl. They have also used this geometry for residual stress measurements in these bond coats and reported a tensile residual stress of 1.55 GPa in the as-deposited condition. Jaya et al.[83] proposed a new doubly clamped beam bend geometry for the fracture toughness determination across individual zones of the bond coat (Figure 1 b). This geometry, being more stable than the single cantilever ones, was used to arrest crack growth and observe crack trajectories post-failure. Their study reported a sharp rise in K$_{IC}$ from 5 to 20 MPa.m$^{1/2}$ with increasing Ni : Al ratio across the thickness of the graded PtAl bond coat. A direct comparison of the K$_{IC}$ values reported by Webler et al.[84] and Jaya et al.[83] does not seem prudent due to the difference in sizes of the specimens used in the above studies and the attendant difference in microstructural features contained in these specimens. While the beam dimensions used by Webler et al. covered only single crystals of NiAl in the bond coat, the beam dimensions used by Jaya et al. were larger and spanned at least 8–10 NiAl grains. In that sense, the K$_{IC}$ value reported by Webler et al. was more that of single crystal NiAl while the K$_{IC}$ value captured by Jaya et al. was that of polycrystalline NiAl and representative behaviour of bond coats. Nevertheless, based on the fracture properties reported in the above studies, it can be clearly ascertained that the natural compositional as well as microstructural gradients that appear in the diffusion aluminide bond coats are beneficial in providing a rising fracture toughness which enables crack arrest and, thereby, prevents catastrophic failure. It needs to be mentioned that these K$_{IC}$ values are from room temperature measurements and high temperature fracture behaviour in the PtAl bond coats is yet to be studied at this size scale.

Miniaturized disc bend testing (MDBT) has been used by Eskner et al.[55] to evaluate the fracture properties of as-deposited and oxidized overlay MCrAlY coatings (Figure 3). The elastic modulus of the oxidized MCrAlY coating was higher than that of as-deposited coating while their yield strengths were similar. Further, shearing of inter-splat regions and plastic deformation of splats were identified as the respective deformation mechanisms in the APS deposited MCrAlY coating at temperatures below 500°C and beyond 650°C. Eskner et al. also evaluated the BDTT and fracture behaviour of a diffusion aluminide bond coat using the MDBT method. The BDTT, determined as the temperature corresponding to the change in slope in the strain-to-fracture versus temperature plots was reported to be about 800°C. They also carried out fractographic studies and reported that the mode of fracture in the coating at temperatures below and above the BDTT was transgranular and intergranular respectively.

Variants of bend test technique, to a limited extent, have been adopted to evaluate the mechanical properties of the ceramic YSZ top coat. Blister tests were used by Zhou et al.[85] to determine the elastic properties of the coating and interfacial fracture properties between the bond coat and top coat, accounting for the residual stresses in the coating. They report a fracture toughness of 0.7–1.5 MPa.m$^{1/2}$ for the interface and showed a small dependence on phase angle. Arai et al.[86] used a bi-axial fracture testing device to apply increasing mode mixity in the APS-coated specimen carrying an interface crack. The geometry was very similar to an asymmetric double cantilever beam, with one of the beams pulled away from the other, at increasing phase angles. Interfacial fracture energy at large phase angles was 2–3 times higher than in mode I and this difference was attributed to contact shielding due to the rough fracture surfaces rubbing against each other. Eberl et al.[87] have characterized the interfacial fracture toughness between a MCoCrAlY bond coat and YSZ top coat using end-supported micro-beams machined via micro-EDM and loaded in three and four point bending in mixed mode. This method can extract material properties of individual layers of the coating, without isolating them and also alleviates the effect of residual stress on the measured toughness values. They used a custom built load frame and DIC for displacement and strain measurements. The setup was used in combination with inverse FEM code to calculate both the tensile properties of the top coat and crack opening displacements along the bond coat-top coat interface. An in-plane elastic modulus of 15–30 GPa and a tensile strain to failure of 3.5–5×10^{-3} was recorded for the EB-PVD deposited YSZ layer[88]. They reported a delamination toughness rising from 25 to 95 J/m^2 with increasing crack length[89]. Similar adhesion energies were calculated by Thery et al.[90] using four point bending of symmetrical interfacial cracks between a β-NiAl bond coat and columnar YSZ

top coat. Liu et al.[91] have recently carried out micro-beam bend tests on vertical cantilevers of the APS-TBC top coat and reported fracture toughness values of 5 MPa.m$^{1/2}$ along splat interfaces, which is at the higher end of the known fracture toughness range for bulk YSZ.

(iii) *Micro-tensile testing*: Pan et al.[33] demonstrated the use of micro-tensile testing technique for evaluating the tensile behaviour of a low activity PtAl bond coat. Free-standing PtAl coating micro-specimens were fabricated from a TBC system using a combination of sinking EDM and precision polishing techniques. The micro-specimens were flat with triangular ends and a rectangular gauge section. As the PtAl coating micro-specimens are brittle, grips having triangular grooves matching the ends of the specimens, i.e. slotted grips, were used for holding the specimens during the tensile tests. Tensile testing was carried out at various temperatures ranging between room temperature (RT) to 1200°C and at a strain rate of 10^{-4} s^{-1}. Strain in the specimens during tensile deformation was measured *in-situ* using an interferometric strain displacement gauge (ISDG). The stress–strain response of the coating was linear and the plastic strain negligible at low temperatures, indicating brittle fracture characteristics in the coating. Plastic deformation or yielding, indicated by onset of deviation from linearity in the stress–strain curves, was observed at temperatures of 600°C and above (Figure 5). The BDTT of the coating was determined to be 600°C where yielding in the coating began. The elastic modulus of the PtAl bond coat at RT was 117 GPa and decreased with increase in temperature in a linear fashion, obeying the empirical relation E[GPa] = 118–0.024 T [°C]. For temperatures below BDTT (600°C), where the coating failed in a brittle manner without any yielding, the fracture strength of the coating increased from 100 MPa at RT to about 330 MPa at 500°C. Above BDTT, however, the yield strength of the coating decreased with temperature from a value of 230 MPa at 650°C to about 25 MPa at 1150°C. The flow strength of the PtAl bond coat was sensitive to variation in strain rate. At 700°C, the flow strength increased from about 20 MPa to 130 MPa with increase in strain rate from 10^{-4} s^{-1} to 10^{-3} s^{-1}. The effect of cyclic oxidation on the tensile behaviour of low activity PtAl bond coat was also studied by Pan et al.[33]. The oxidized coating exhibited similar stress–strain behaviour as that observed in the as-deposited coating, i.e. the stress–strain response was linear at temperatures below BDTT while yielding was observed above BDTT. The room temperature elastic modulus for the oxidized coating was about 50% higher than that of the as-deposited coating. Further, the yield strength of the oxidized coating was higher than that of the un-oxidized coating. The BDTT of the oxidized coating, however, was similar to that of the un-oxidized coating. By carrying out stress-relaxation tests at elevated temperatures, Pan et al. gave a power law description to
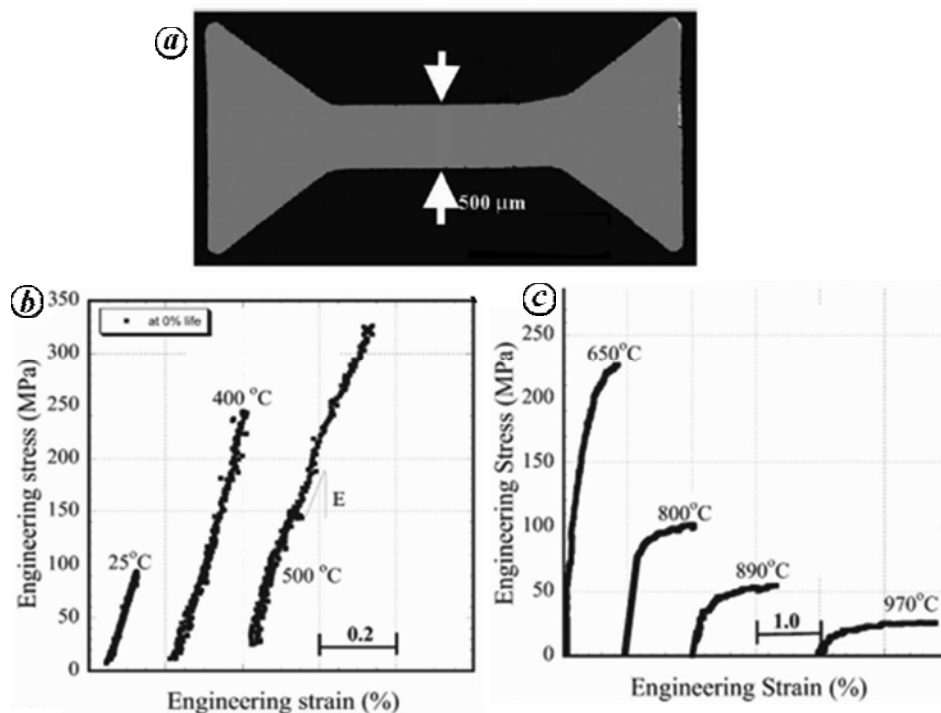
Figure 5. *a*, Mini-tensile sample of PtNiAl bond coat; *b–c*, Stress–strain response of the free-standing low activity PtAl coating at various temperatures[33]. The strain rate of testing was 10^{-4} s^{-1}.

the creep behaviour of the PtAl coating. Further, they reported a rapid decrease in creep strength with temperature. Based on strain measurements, carried out on un-strained coating specimens using IDSG, they also recorded an increase in CTE from 14.5 to 16.5×10^{-6}/°C for the PtAl bond coat. Micro-tensile testing method was also adapted by Alam *et al.* to evaluate the tensile behaviour of free-standing high activity PtAl bond coats at various temperatures and strain rates in the range RT-1100°C and 10^{-5}–10^{-1} s^{-1} respectively[44]. Flat tensile specimens with rectangular ends, designed using a FEM-based approach, were used in their study[92,93]. The free-standing coating specimens were fabricated using a combination of precision wire-EDM and polishing techniques[44,92]. Slotted grips were used for holding the specimen during the test while the *in-situ* strain in the specimen was recorded by a non-contact video extensometer. High temperature in the specimen was achieved using impressed DC current while the temperature was monitored using a radiation pyrometer. At all strain rates, the stress–strain response for the PtAl coatings was linear, indicating brittle fracture up to about 700°C while ductile failure marked by yielding was observed at high temperatures. The elastic modulus and the strength (YS/UTS) of the coating decreased with increase in temperature. On the other hand, increase in strain rate caused an increase in fracture stress and strength (YS/UTS) while the elastic modulus remained more or less unaffected. The BDTT of the coating was reported to increase

appreciably by about 400°C with increase in strain rate of testing from 10^{-5} to 10^{-1} s^{-1}. Alam *et al.* also carried out extensive post-deformation SEM as well as TEM analyses of these specimens and proposed detailed micro-mechanisms involved in the deformation of these coatings at temperatures below BDTT, in its vicinity and above it[93]. The effect of Pt content on the tensile behaviour of stand-alone PtAl coatings in the temperature RT-1100°C was also evaluated by Alam *et al.* The elastic modulus of the coating decreased while the fracture stress, strength (YS/UTS) and BDTT increased with increase in Pt content. Based on the TEM analyses of deformation sub-structure, the parameters contributing to the strength in the coatings at various temperatures were ascertained and quantified.

Mechanical properties of Si-based MEMS systems

Si (and its associated silicides, nitrides and oxides) has emerged as the 'go to' structural material for MEMS, micro-robotics and micro-electronics industry due to its easy availability, low cost, high purity, semiconductor properties, ability to be cast into extremely thin single crystal wafers and machinability. As increasing number of devices are being churned out every year on Si substrates, going by Moore's law, increasing miniaturization follows suit. Not only does the elastic response of Si directly affect the functioning of devices like gyroscopes,

optical switches and micro-mirrors, but the reliability and durability of these components rests on the fatigue and fracture behaviour of the underlying Si substrate, which is a known brittle material. Fracture properties of brittle systems are governed by flaws at the surface and interior, which in turn depend on the processing condition. Also the approach in determination of fracture strength in such structures is probabilistic in nature, given the scatter in the number, nature and distribution of flaws in them. In addition to the known elastic anisotropy of Si, a large scatter in the reported values of elastic modulus of poly-Si from 90 to 190 GPa is sufficient to underline the urgent need to systematically characterize these specimens for their mechanical behaviour[94]. The mechanical response of thin film specimens is affected more by the size (thickness) than the microstructure as free surface effects begin to dominate when the specimen is constrained along one dimension in thickness[95]. Transport properties like electrical and thermal conductivity also undergo changes when the specimen thickness is reduced beyond the mean-free path of electron and phonons[96]. Si-based structures are also prone to failure by fatigue, wear and stiction. Direct evaluation of the structure every time a product is rolled out is expensive and can be done away with by modelling and simulation of such structures, but it requires using the actual material properties at these size scales for reliable prediction of their behaviour in the end product. Several novel techniques for mechanical property determination of Si films have emerged: bulge tests, cantilever bend tests, laser-acoustic techniques, AFM-based tests, on-chip MEMS tests and many others. Here we summarize the known results from various techniques while highlighting the dependence of measured properties on the test method and what else needs to be done to determine the true material property from these specimens.

(i) *Fracture*: Fracture strengths of Si-based structures have been found mainly by cantilever bending or micro-tensile tests driven by thermal or piezoelectric loading. A round robin of tensile tests carried out on co-fabricated poly-Si specimen have all shown the tensile strength of poly-Si to reach nearly theoretical values, varying anywhere between 1 and 4 GPa (refs 97–99). The wide scatter recorded depends not only on the intrinsic factors of poly-Si such as microstructure, processing conditions, flaw distribution and residual stress, but also on extrinsic factors like loading type, layout, geometry and specimen size. The mono-crystalline Si films themselves show fracture stresses anywhere between 1 and 20 GPa (refs 100–102). Hence, the reliability calculations for the device using these values directly become impossible. The fracture toughness values also show considerable variation, with recorded values anywhere between 0.9 and 4.5 MPa.m$^{1/2}$ (refs 101–106). Notches were introduced by different means in each of these cases-RIE, indentation or FIB, all

of which induce artifacts in the measurement due to the finite tip radius which in turn leads to over estimation of strength as blunt notches replace sharp pre-existing cracks.

Ding et al.[96] carried out micro-cantilever deflections of poly-Si specimen of average grain size 200 nm using a nano-indenter and found a size effect in rupture strengths with a decrease in strength with increase in specimen volume and decrease in surface area whereas the Young's modulus remained unaffected and was constant at ~156 GPa. The critical size of the flaw driving their fracture was the same order as the surface roughness of these cantilevers. In a counter intuitive result, they showed that the rupture strength increased with increasing surface to volume ratio of the specimen whereas it decreased for increasing effective volume. Boroch et al.[107] used the Weibull scheme to calculate fracture strengths of poly-Si specimen of varying cross-sections in four different geometries produced by Bosch mass production micro-mechanical process and used the same in predicting failure in more complex geometries. The fracture strengths showed both a size and geometry dependence while fracture toughness was independent of the specimen size. Namazu et al.[108] determined the fracture strengths of a wide size range of Si wafers, starting from the sub-micron scale all the way to the millimeter scale, and found a 37 times increase from 0.47 to 17.5 GPa with decreasing size scale. Son et al.[101] determined fracture strengths of single and polycrystalline Si films using micro-tensile tests and found a dependence on both geometry and doping conditions. The samples were prepared by surface micro-machining and gripped using a UV adhesive and tested by alternating electrostatic force. They introduced fatigue pre-cracks using electrostatic resonance and found the fracture toughness of notched specimen with a notch radius of ~1.4 μm to be 33% higher than that of pre-cracked specimen, although these values were geometry independent. They used the AFM to evaluate the surface topography of these structures on the dry-etched side and chemo-mechanically polished side and found a lower failure strength on the dry-etched side with a higher surface roughness and larger detectable surface flaws. Bagdahn et al.[105] also compared the fracture toughness of poly-Si obtained from indenter pre-cracks and FIB machined notches in tension and bending to find a higher K_{IC} in FIB notched samples. Unusually, they also found a fracture toughness of 1.1 MPa.m$^{1/2}$ in bending vis-à-vis 2.15 MPa.m$^{1/2}$ in tension, showing a dependence on the loading mode. They attribute this to the effect of the notch quality and hence to the FIB process of manufacturing of the sample which leaves residual re-depositions at the notch, acting as bridges between notch walls. Ga ion implantation is also speculated to affect the micro-structure of poly-Si at the notch tip, driving such property changes. A stable double cantilever geometry was used to measure the notch toughness of micron sized Si fabri-

cated by DRIE, where in a wide scatter was found in K_{IC} between 0.9 and 1.65 MPa.m$^{1/2}$ (ref. 109). Ando *et al.*[104] carried out fracture toughness measurements of single crystal Si thin films and found a dependence of K_{IC} on loading direction (1.94 MPa.m$^{1/2}$ along <100> and 1.17 MPa.m$^{1/2}$ along <110> while they were free from the influence of surface orientation. In comparison to known values of K_{IC} of bulk Si (0.7–1 MPa.m$^{1/2}$) obtained via indentation methods[110], these values were higher, pointing to a possible size effect in the fracture toughness of these micron-sized specimens. Correspondingly, the fracture surfaces and crack trajectory in the two orientations were different for the micron-sized specimens, while they claimed that there was no recorded orientation dependence of K_{IC} in bulk Si. Li *et al.*[111] carried out similar set of experiments on-chip using FIB notched (110) and (001) Si thin films with different tensile orientations as shown in Figure 6 and reported a fracture toughness variation of 1 to 2 MPa.m$^{1/2}$. They also saw a dependence of the inclination angle of the low index plane relative to specimen surface affecting the fracture path in these specimens.

(ii) *Fatigue*: With both alternating stresses and notches routinely present in MEMS structures, the fatigue behaviour of these components becomes equally important. Alsem *et al.*[112] have put together a review, compiling various results and mechanisms proposed for fatigue failure of micron-scale Si films. The results for single and polycrystalline films are shown in Figure 7. Though bulk Si is not known to be susceptible to fatigue failure or to stress corrosion cracking[113], Si films are reported to be prone to fatigue failure and stress corrosion cracking. Fatigue loading at micron scale and below is carried out either using on-chip electrically actuated systems (micro-resonators, electrostatic actuators and comb drives) or externally actuated systems (piezo-actuated resonators, electro-magnetic resonators, AFM actuators or load lever and torsion bar combinations). Reliability measurements have been done using cyclic loading experiments on both
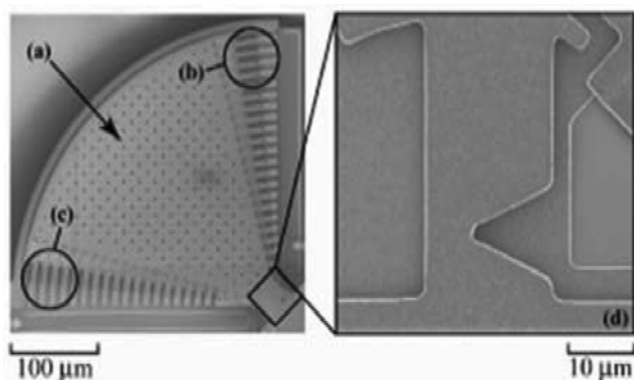
Figure 6. MEMS-based fracture toughness testing specimen in Si[122].

notched and un-notched specimens wherein, it is observed that fatigue strengths decrease rapidly with increasing number of cycles[114–116]. Muhlstein *et al.* found a 50% drop in fatigue strength in 10^9–10^{11} cycles[117]. A common observation made in all the fatigue tests was a dependence of fatigue life on the humidity/dryness of the loading environment[116]. Cyclically loaded samples exposed to higher relative humidity or ambient air showed lower fatigue life compared to those in dry air or vacuum conditions pointing to environmentally assisted cracking. Alsem *et al.*[118] carried out fatigue tests on resonator poly-Si specimens and confirmed the occurrence of cyclic stress-assisted oxidation using high voltage transmission electron microscope (HVTEM). Also, all the tests showed a distinct independence of fatigue strength and number of cycles to failure from loading frequency[105], indicating that it was not merely stress corrosion cracking that was playing a role because then the time to failure would be constant irrespective of the frequency of loading. Two different viewpoints on the fatigue failure mechanism in micron-scale Si are currently in place. Kahn *et al.*[119] suggest sub-critical cracking in the Si itself as the driving mechanism for cyclic failure in these specimens whereas Muhlstein *et al.*[117] have proposed reaction layer fatigue process wherein the cracking of the native SiO_2 scale covering the Si structure actually causes damage accumulation and drives fatigue failure. There is more experimental evidence to support the latter mechanism. Neither micro-cracking nor enhanced dislocation activity at crack tips has been observed on Si structures under the TEM[120]. The sub-critical cracking of the oxide scale due to moisture-induced reaction and its propagation and arrest at the SiO_2–Si interface before unstable fracture ensues in the Si, is able to explain correctly many of the observed results including the absence of fatigue failure in bulk specimens. TEM studies have revealed a thickening of the oxide layer at the highly stressed notch root regions, suggesting a stress driven mechanism contributing to the same[121,122]. While the oxide thickness remained at ~30 nm for the control specimen and monotonically loaded specimen, the notch root of the cyclically loaded specimen had a thickened oxide layer of ~90 nm with several stable small cracks in them. The IR imaging showed the temperature rise to be minimal during the loading, strongly suggesting that the oxide growth occurred due to mechanical rather than thermal reasons. AFM measurements of surface topography also show an increased roughening of the surface near the stressed portions like in the immediate vicinity of the notch root, again indicating selective growth of the oxide scale in these portions[123]. These have been accompanied by a decrease in resonance frequency of the loaded structures indicating slow crack growth[122]. The drop in resonance frequency fits well with the measured crack length in the oxide scale. The compressive residual stresses that develop during oxide growth experience two opposing stresses
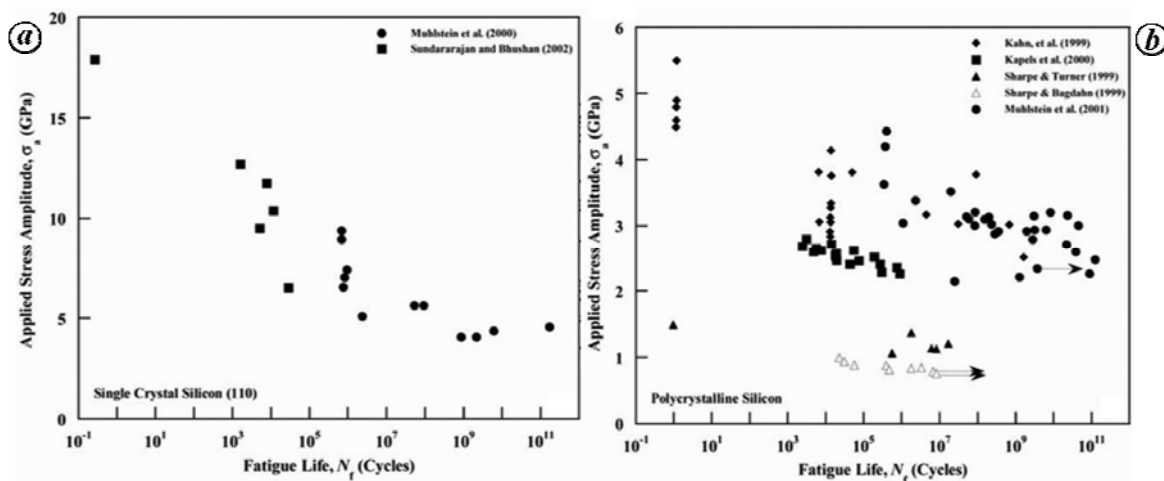
Figure 7. Fatigue life determined by various research groups in (*a*) single crystalline and (*b*) poly-crystalline Si[112].
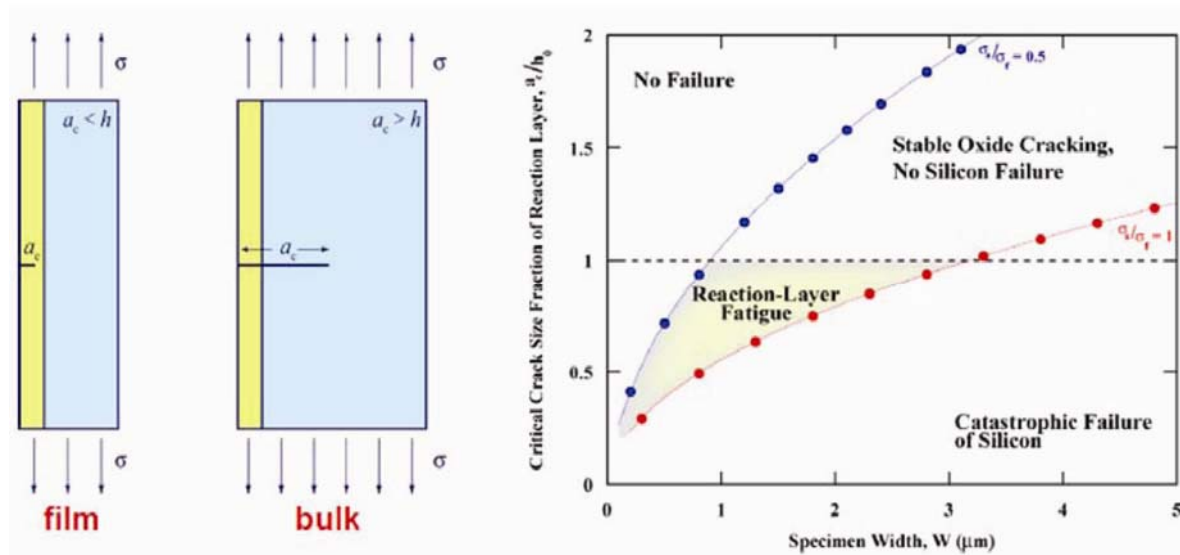

Figure 8. Fatigue–fracture map in Si thin film systems showing domains of critical film thickness beyond which catastrophic fracture precedes fatigue failure[121].

during cyclic loading, bringing about a change in the oxide growth rate, both due to relief of intrinsic stresses and enhancement of driving force for growth at the Si–SiO$_2$ interface. Muhlstein *et al.*[124] have provided a fatigue failure map for thin film structures showing the critical oxide thickness vis-à-vis applied stress, clearly distinguishing domains of no cracking and sub-critical cracking as safe zones and reaction layer fatigue, as responsible for final failure (Figure 8). In thin films, the critical crack length required for device failure is less than the oxide layer thickness, which is why delayed failure becomes possible. Coating the Si using alkene based SAM has been seem to arrest fatigue failure and increase fatigue life by orders of magnitude[122], giving credence to the belief that inhibition of the oxide scale formation using barrier layers can improve the fatigue resistance of these structures.

There have been some more unusual results from compression experiments of Si nano-spheres and pillars that are worth a mention before closing this section. Gerberich *et al.*[125] interrogated defect free Si nano-particles, 20–50 nm in size in a SPM based nano-indenter. They found hardness values up to 50 GPa, prompting the authors to call them superhard nano-spheres. They used molecular dynamics simulations to explain the dislocation loop evolution in Si structures. Deneen *et al.*[126] compressed individual nano-particles of Si between a diamond tip and sapphire substrate inside the TEM to study their deformation behaviour. They observed substantial plastic deformation in these spheres before failure. They also calculated the surface energies of contacting spheres using contact mechanics theory. Lockwood *et al.*[127] carried out *in-situ* TEM compression experiments of ~50 nm Si nanoparticle clusters using a W-indenter tip

and found localized orientation changes in individual particles before the cluster failed along a weak interface between two nano-particles. The cluster took up a contact pressure of 17.6 GPa before failure. Deformation and plasticity in nano-scale Si have been modelled using molecular dynamics simulations[128]. A critical size of Si nanoparticle has been proposed for initiating the change in deformation mechanism via a phase transformation from diamond cubic to β-tin structure. Ostlund et al.[129] found a brittle to ductile transition in Si at room temperature under uniaxial compression for pillars smaller than 300 nm. The mechanism for such a transition is still unclear and requires detailed TEM studies, but proposed mechanisms involve the widely separated shuffle dislocations at the high stresses that these smaller pillars experience or the much closer glide set whose equilibrium spacing is larger than the pillar size due to which a single partial glides through the entire cross-section without nucleating the trailing partial.

Biological systems

The importance of determining the mechanical behaviour of biological specimens is increasingly being realized for a variety of reasons: they are constantly exposed to stresses and strains in both external and internal environments which causes their failure due to fatigue and fracture. Protein molecules responsible for such responses can be identified and modelled to develop lifetime predictive capabilities with respect to health, disease and age. Bio-mechanical response of a diseased cell is different from a healthy cell and is a manifestation of its molecular structure and organization, which in turn governs its movement, deformability, adaptation and multiplication[130]. Any deviation in the structural and mechanical properties results in disruption of functional capabilities. Modification and control of bio-mechanical properties can be achieved by introduction of chemical or pharmaceutical agents enabling therapeutic treatment of diseases. The exo-skeleton of many animals is designed by years of evolution to be optimized for the highest strength to weight ratio to take up compression, bending or tensile loads. Hierarchical structures like nacre and bones, spider silk as well as gecko's feet are being mimicked for their excellent mechanical properties (biomimetics). Popular testing apparatus for manipulation of biological systems *in vitro* include the AFM, optical tweezers (nano-scale-DNA and viruses), nano-indentation, micropipette aspiration and micromanipulators (micro-scale-RBCs, tissues) and molecular force spectroscopy. Lim et al.[65] have reviewed the instrumentation and techniques of testing of features as small as single cells/molecules whereas Meyers et al.[130] have given a detailed compilation of well-known mechanical properties of various biological structures at different length scales starting from cells to

organs. Out of studies on diverse biological systems, two are described here as case studies.

Biological cells: Suresh and co-workers have studied the bio-mechanics and bio-physics of cells causing cancer, malaria and sickle cell anaemia and clearly established the connection between cell architecture and cell mechanics and their implications on disease diagnostics and treatment[131,132]. A healthy human red blood cell (RBC) is highly deformable, transforming from a bio-concave to a bullet shape while travelling through narrow capillaries less than half its diameter and completely recovering its original shape after flow. An RBC infected with malaria causing virus or in case of sickle cell anaemia loses its elasticity and hardens, impairing its flow in the body. Suresh et al.[131] have shown using optical tweezer experiments on living RBCs in healthy and infected conditions that RBCs in diseased condition show a 10 times increase in shear modulus compared to normal cells. They have carried out tests on cells infested with two different malaria-causing parasites at different stages of infestation. These are correlated to the bio-chemical condition of the parasite containing cell to draw implications on disease pathogenesis. They postulate that stiffening is caused by the transport of specific proteins from the plasmodium parasite to the cell membrane or cytoskeleton. As a part of the same paper, they have discussed the mobility of pancreatic cancer cells and its relation to cell structure and effect on disease progression and meta-stasis when treated with different biochemical agents. They have repeatedly loaded the cells in tension in both load and displacement control using a mechanical micro-plate stretcher and compared the energy dissipation and modulus of the cancer affected cell treated with various agents. Cell migration and proliferation go hand in hand in the spread of cancer and the cells treated with one set of chemicals, sphingosyl-phosphoryl-choline (SPC), a bio-active lipid naturally found in parts of the human body (which alters the peri-nuclear reorganization of keratin fibers), is found to be responsible for the same. This is reflected as a 3-fold reduction in elastic modulus and increased dissipation and hysteresis with fatigue cycles in SPC-treated cells, increasing the ease of cell locomotion and facilitating their spread by squeezing through size limited pores. Many such cell and protein structures are being studied today by various techniques (Figure 9) and the relevance of their mechanical properties on their functionality is to be established.

Nacre-mechanical properties: Nacre shells (abalone) consist of a periodic and highly textured structure of aragonite, the orthorhombic form of $CaCO_3$, arranged in staggered layers over multiple hierarchies all the way from the nano to meso-scale, with a proteinaceous organic layer in between[130]. This arrangement is popular as the brick (aragonite) and mortar (protein) structure and is
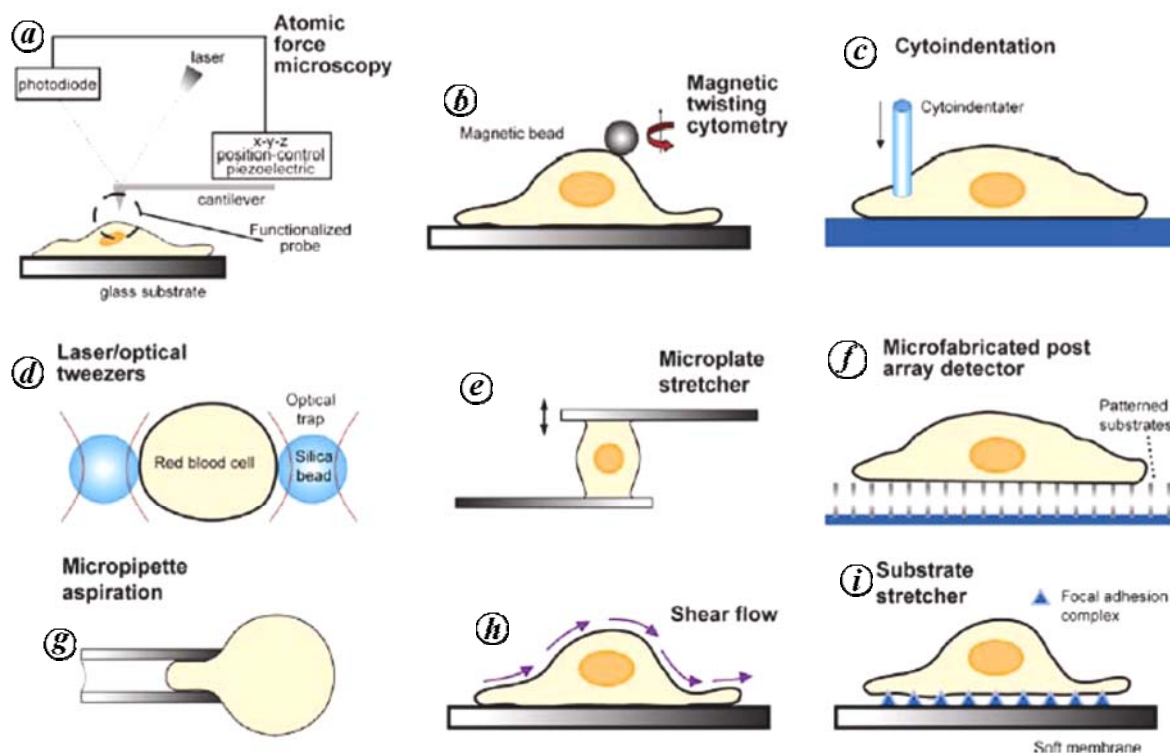
Figure 9. Schematic of various methods of biological specimen testing at the molecular and cellular level[186].
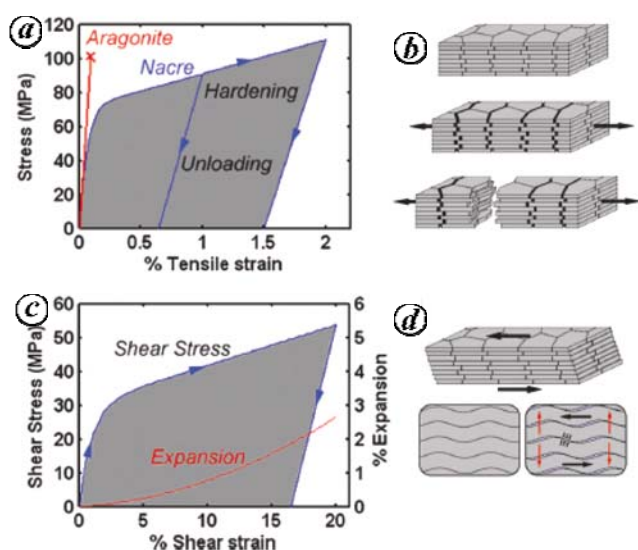

Figure 10. Nacre tested in both (*a*) tension and (*c*) shear. (*b*) and (*d*) refer to deformation mechanism in the two testing modes[133].

responsible for the high impact and fracture resistance of shells despite 95 wt% of abalone having been made of the brittle mineral phase. Various models have been proposed for the organic phase which itself possesses a structure and is not a single phase[133]. A remarkable consistency in dimensions at every stage of the hierarchy is also a highlight of such shell structures.

Many different approaches have been followed for determination of mechanical properties of such structures till date. Nano-indentation studies have been carried out on single nacre tablets[134,135] while P–h responses have been obtained from single molecules of organic materials[136]. But Oyen[137] has cast doubts regarding the validity of such measurements due to the lack of straightforward analysis of indentation data, especially when involving visco-elastic, soft material response of the ceramic–polymer composite combine as compared to the linear, elastic, homogeneous material behaviour for which indentation was developed originally. It is now well known that these highly ordered bio-composites show a work of fracture and fracture toughness that is 3000 times and 8 times higher respectively, than their principal constituent, the monolithic $CaCO_3$; the crack propagation showing a high degree of tortuosity[138,139]. The ratio of compressive to tensile strength perpendicular to the tiles was found to be 100, while in the parallel direction it was about 2 to 3 compared to 8–10 found in conventional ceramics[140], thereby showing a high degree of anisotropy. The relatively large tensile ductility of up to 2%, parallel to the layers as shown in Figure 10, is explained by the yielding of the organic layer at the interface and shearing of the aragonite tablets on one another before the fibers pull-out and ultimate failure ensues[133]. The requirements for such sliding in tension are: an interface which has a strong adhesion to the tablets, a high enough aspect ratio of the mineral tablets and a hardening mechanism at the local

scale to spread the deformation throughout the material. Nano-asperities on the tablet surface can enhance friction and provide some strengthening by inter-locking[141].

Complete fracture resistance curves have only recently been determined by miniaturized fracture toughness tests on abalone nacre[142]. Stable cracking and a rising R-curve is found for these shells as against catastrophic failure of conventional ceramics. Extensive inelastic deformation occurs, as reflected in the whitening ahead of the crack tip, showing a process zone formation. Both plastic micro-buckling and crack deflection in meso- and micro-scale have been found to be responsible for the enhanced toughening in these structures[142] while sliding and ligament formation have also been proposed to play an important role[143]. The source of the enhanced fracture resistance still remains a matter of debate. This calls for testing such hierarchical structures at different length scales to determine the toughening mechanism at each stage.

Such architectures were successfully mimicked in many ceramic–ceramic, metal–ceramic and organic–inorganic composite systems. Sequential deposition of organic poly-diallyl-dimethyl-ammonium chloride (PDDA) and inorganic (clay) layers was carried out by Tang et al. by a layer-by-layer assembly process, achieving characteristic dimensions three times smaller than that of nacre[144]. The stress–strain behaviour of these multilayer systems was very different from that of nacre and relied on the electrostatic attraction between the constituent particles, limiting its use to only a certain class of materials. Poly-Si and photoresist have been used in another recent work to create three-layered micro-composite structures mimicking conch shells, using standard MEMS technology and RIE[145]. A 36 times increase in energy dissipation was recorded compared to Si, though the toughening process was different from that of mollusc shell. Brick and mortar structures of Zr–ZrN multilayers were made by heat treatment by Verma et al.[146] although a thorough investigation of the mechanical property enhancement is yet to be made in this case.

Residual stress determination in thin films

Thin film growth is often accompanied by growth stresses due to lattice mismatch, grain boundary formation, thermal mismatch and diffusion and grain growth[11]. Stoney proposed a formula for measurement of thin film stress when attached to a much thicker substrate[53]. Ex-situ post-growth studies of such residual stresses by XRD or laser curvature experiments are possible though information is lost due to post-deposition stress relaxation. Such stresses can be measured in-situ by multi-beam optical stress sensors (MOSS) during the thin film deposition process itself, without bringing about any damage to the coating (Figure 11)[147]. The MOSS system consists of a single beam laser that is split into parallel arrays by

an etalon and this array is reflected off the growth surface of the film. Gas purged optical ports are used for the entry and exit of the laser array. Both the beam spacing and intensity are monitored during the thin film growth using a CCD camera interfaced with a computer. Any change in the stress level is reflected in the thin film curvature, which in turn brings a change in the beam spacing. This is then put in as an input in the Stoney's equation to calculate the film stress. The spot intensity provides useful information regarding thickness and surface roughness evolution. Both the growth rate and optical constants can be extracted from the oscillation frequency of the laser intensity versus time plot, gathered using a virtual interface model. One of the systems in which this technique has been applied to significant use is that of GaN thin films on Si-based substrates[148]. Stress thickness versus GaN film thickness is plotted to determine stress evolution in these systems.

GaN and its alloys are useful in opto-electronic devices like light-emitting diodes where epitaxial multilayers of GaN/AlGaN or InGaN/GaN produce bright light over an entire spectrum of colours. But the device efficiency depends on the minimization of dislocations, which act as non-radiative recombination centers. This is one illustration of how the microstructure of a material can control its functional behaviour. Other problems persist during thin film growth, for example cracking in AlN/GaN layers on Si substrate; delamination in InN; pit formation in AlGaN and InN systems and grain boundaries in all cases[148,149]. Misfit dislocations are invariably produced on growing films above a critical thickness, as that is the only means of plastically relaxing stresses. This is especially true in hetero-epitaxy, where a thin layer is grown on a substrate with significant lattice parameter difference. Such stresses are minimized or compensated by various techniques, including use of a buffer AlN layer[150] and that of a graded AlGaN layer[151] to induce compressive stresses to overcome the tensile residual stresses that occur during cool down. This helps prevent cracking to an extent and also minimizes threading dislocations in the system. Several ex-situ techniques like XRD, TEM, wafer curvature, Raman and photoluminescence were previously used in determination of stresses in these films[152–154] but they were unable explain the exact growth mechanism. They also lead to different conclusions, reporting stress values different from those predicted due to thermal expansion mismatch. Stress state at the growth temperatures was left to mere speculation. Hearne et al.[150] were the first to show by in-situ wafer curvature measurements that GaN grows in tension, independent of the buffer layer. Later, growth stresses in both AlN buffer layer and GaN layers grown by MOCVD were measured in-situ and in combination with TEM studies were used to correlate the same to structural evolution during thin film growth[155]. Dislocation evolution was seen to occur only under the influence of compressive stress in the film. On
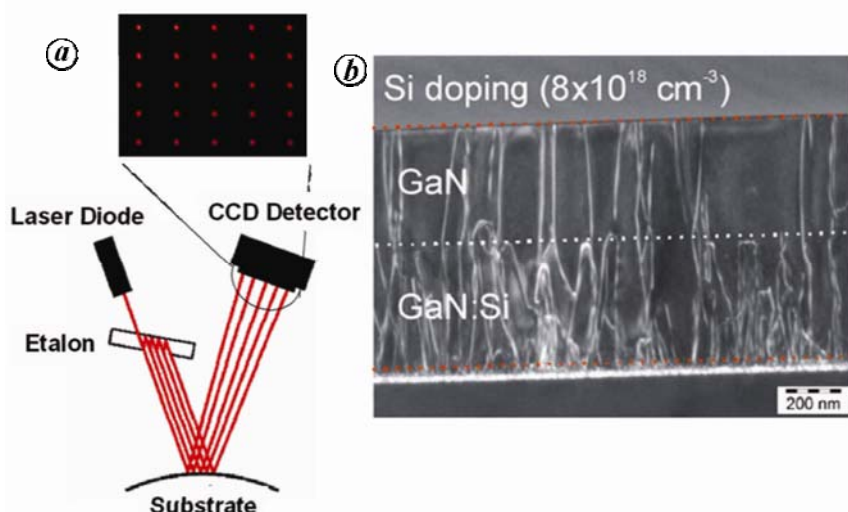
Figure 11. *In-situ* residual stress measurement of thin film by multi-beam optical stress sensor (courtesy: K-space Associates, Michigan) and dislocation structure evolution in undoped and doped GaN as seen inside the TEM[187].

the basis of his observations, Raghavan[156] proposed a kinetic model for dislocation bending at the growth surface in compressively stressed, low mobility films like III–V nitrides. Krost et al.[149] also used the same technique to study the effect of a number of variables like epitaxial and thermal mismatch, dopant additions, and 3-D island coalescence on the integrity of the hetero-epitaxial structure of group-III nitrides on Si substrates. They developed relevant numerical expressions for cases where the wafer bending is larger than the limit specified by Stoney's formula. This would account for errors resulting in the measured mismatch strains when the linear approximation of Stoney is used. Lee et al.[157] determined the critical thickness for strain relaxation in GaN/AlGaN layers using *in-situ* wafer curvature measurements and AFM. They found evidence of surface cracking preceding formation of misfit dislocations in these heterostructures. Humphrey's group has carried out extensive research on these systems using wafer curvature, TEM and AFM, which has helped gain insights into their growth mechanism and enumerated equilibrium critical thickness for misfit dislocations in a number of group-III nitrides by combining experimental measurements of high resolution XRD and TEM with atomistic calculations of dislocation core energies[158]. Holec[159] proposed a modified critical thickness model to fit InGaN/GaN systems. Such studies show the relevance of *in-situ* stress measurement methods for achieving thick, device quality GaN structures on Si.

Size effect on structural properties

Scaling laws have always been the basis of design in civil, mechanical and aerospace engineering, where geometrically similar structures are compared. Behaviour of laboratory specimen has to be scaled up (e.g., in concrete) or scaled down (e.g., MEMS) to material behaviour at the service point. Power scaling, which is independent of any characteristic size scale, applies to failure theories in continuum mechanics, like elasticity with a strength limit, plasticity and LEFM[160]. In such cases, all geometrically similar structures must fail at the same nominal stress but it is increasingly observed to be not true especially in small structures. In addition to the microstructural length scales like grain size, inclusion or precipitate distribution bringing about the 'intrinsic' size effect, and whose dimensional relation to various material properties is fairly known as of today, it is seen that the external dimensions of the component or device itself play a role, modifying the scaling laws in what is termed as the extrinsic size effect. There is a body of work today on both experimental and computations observations of both types of size effects working in tandem in materials ranging from brittle Si to amorphous glasses, hard coatings to metallic foils and thin films to lamellae tested in tension, compression and bending. There have also been many reviews on this topic, notably from Arzt[95], Dehm et al.[161], Gerberich et al.[162], Greer et al.[9,163] and Gianola and Eberl[19]. One needs to be careful while drawing conclusions about size effects using data of different groups as material strength at small scale becomes sensitive to initial dislocation density or defect structure, which in turn is dependent on the processing and fabrication conditions as well as on other experimental artifacts intrinsic to the geometry of testing such as pillar taper, stiffness of loading/gripping system, sample aspect ratio and ion implantation damage. The stress states associated with the geometries, strain rate of testing and loading condition, i.e. load or displacement control, also have to be taken into consideration when making comparisons. Here we describe the experimental results of size effects on crystalline metals in small structures, which are important both
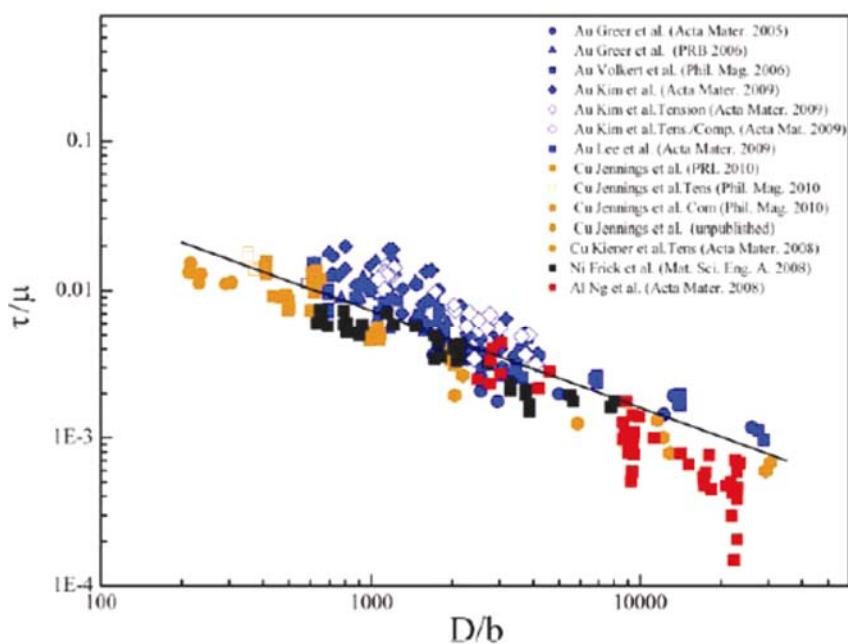
Figure 12. Universal size effect seen in fcc metallic single crystals tested in compression[163].

from point of view of their application and scientific understanding.

Cu, Al, Ag and Ni are structural materials being used today in miniature devices – micro and opto-electronics in the form of thin films, wires, porous structures and interconnects – for their excellent electrical and or thermal conductivity in both single and poly-crystalline form. Various deposition methods are used during their manufacture: PVD, CVD, electro-deposition and sputtering to name a few. Failure of such metallic structures is due to a combination of electro-migration, diffusion, voiding, thermal stresses, corrosion, impurities and defects. Properties like adhesion, strength and fracture become important in such applications. These are the most commonly studied materials for their size effects as their structural stability and strength at the small scale are to be known *apriori* for the development of reliable devices.

Single crystals: Brenner[164] was the first to carry out seminal work on micro-scale whiskers of Ag, Fe and Cu, demonstrating a clear dependence of ultimate tensile strength of these whiskers on their diameter, with the smallest whiskers taking up close to ideal strength of these crystals. A number of groups have since been involved in both *in-situ* and *ex-situ* pillar compression, tension and bend tests of metallic materials in their various forms – as single crystals, nano-crystals, laminates and glasses[163]. A pronounced dependence of strength on specimen size has been found in all cases, albeit differently for different crystal symmetries[9]. For the face centered cubic (fcc) single crystals (Au, Cu, Al and Ni), a universal power law dependence of strength on the characteristic spe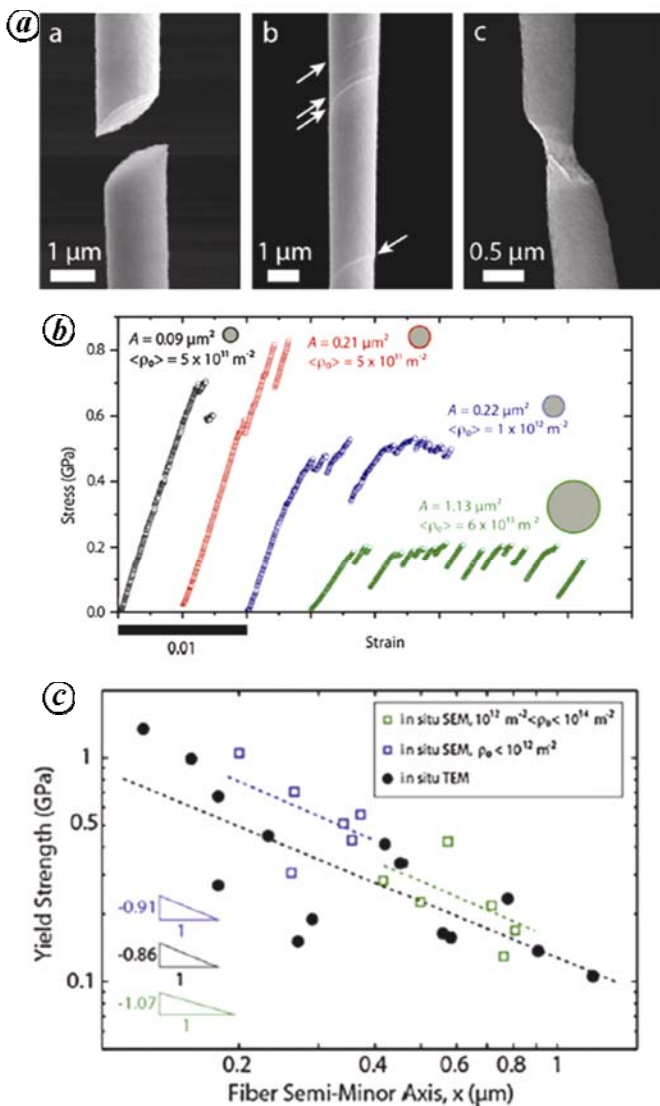cimen dimension has been found, with the power law exponent of –0.6 in uni-axial compression (Figure 12)[163]. A less dramatic size dependence is seen in tension, underlining the need to compare data from similarly stressed specimens[165]. When compared to fcc metals, all of which have a low Peierls barrier, body centered cubic (bcc) single crystals (Mo, Nb, W) with a higher but variable lattice resistance to dislocation motion show a reduced strength dependence on size[163]. They also show a tension–compression asymmetry and orientation dependence of yield strength[9]. It has also been noted that the size dependence is a function of the initial dislocation density in single crystals with pristine metallic nano-whiskers, devoid of initial dislocation structures, showing nearly theoretical strengths to fracture irrespective of their aspect ratio[166]. FIB damage induces finite number of dislocation defects in pillars, due to which they fall short of reaching ideal strengths[167]. Surprisingly, this difference between whiskers and pillars stays even after mechanical annealing of the FIB machined samples to remove the pre-existing dislocations. From extensive *in-situ* SEM and TEM based micro-manipulator tensile experiments on single crystal Al sub-micron wires etched out from an Al eutectic, Mompiou *et al.*[168] found evidence for the exact correlation between the observed size effect and the initial dislocation density (Figure 13). They conclude that dislocation plasticity depends on the activation of spiral sources within these sub-micron crystals and their distance from the free surface. In addition to the number of available sources, the closer the source to the surface, higher was the yield stress. Further dislocation multiplication proceeded without hardening due to the continuous escape of these dislocations to the free surface, despite some back stress from the native oxide over Al with the

elimination being faster for smaller-sized specimen. These experiments showed single crystal fibre behaviour in a domain in between that of pillars and whiskers.
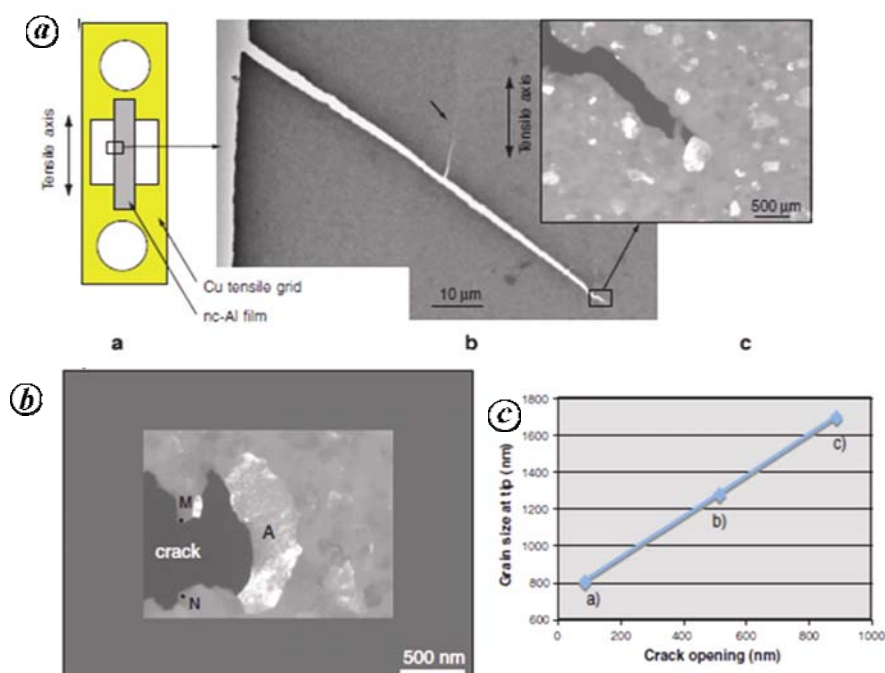
Legros *et al.*[169] based on extensive *in-situ* TEM work of Cu, Al and Ni specimen categorize single crystal flow into three classes, depending on whether they contain a finite to large dislocation density, low dislocation density or are dislocation free. Size effects in flow stress were previously explained using strain gradient plasticity theories based on bending experiments which require geometrically necessary dislocations to explain accommodation of strain[170]. Slip traces in bending are observed only from the surface to the centre of the beam, representing the

Figure 13. SEM observations of deformed fibres after test showing brittle failure, disperse slip lines and necking respectively. *b*, Stress–strain plots obtained for fibres with different sections and average dislocation densities showing a transition from whisker-like behaviour to significantly plastic behaviour with increasing specimen cross-sectional area or dislocation density; *c*, Flow stress obtained from both *in-situ* SEM and *in-situ* TEM experiments as a function of the smallest specimen dimension across the fibre[168].

neutral axis, where pile up of dislocations causes a back stress which inhibits further propagation of dislocations[169]. This effect is pronounced for thinner beams and contrasts with uniaxial tensile testing where slip traces are observed throughout the specimen's cross-section. But since then, pillar compression experiments with no such strain gradients were also seen to exhibit size effects[161]. A number of mechanisms have been proposed for the observed dependence of strength on specimen size for single crystals; most notable among them are: the dislocation starvation model, source truncation and exhaustion, single arm source theory and percolation-based weakest link theory[163]. Each of these models is valid for a particular size range, eluding any universality to these theories. Some of these theories have got backing from molecular dynamics and crystal plasticity simulations as well as from *in-situ* TEM observations during deformation. While compression experiments support the dislocation starvation theories, tensile tests have shown a constant dislocation density throughout their plastic deformation suggesting that the mechanism is dependent on the mode of testing. Results from micro-beam bending experiments were explained by a combination of dislocation starvation and pile-up models, with the neutral axis itself acting as a barrier to dislocation motion resulting in pile up of dislocations, these dislocations; themselves occurring on limited number of slip planes as a result of insufficient number of sources in the shrinking deformed volume[161].

Polycrystals: Strength is also known to be a function of the microstructural length scale like grain size or laminate size. Introducing a grain boundary, as in a bi-crystal, results in smoother deformation, shorter strain bursts and higher flow stresses as compared to its single crystalline counterpart[171]. A larger density of residual dislocations has been found in the boundary containing bi-crystal samples in TEM. There is still disagreement on the 'smaller is stronger' premise for nano-scale, nanocrystalline specimen. Strain accommodation in crystals in the nano grain-regime showing breakdown in the Hall–Petch scaling is explained by a number of mechanisms – grain rotation, grain boundary sliding, partial dislocation emission, twinning, diffusional creep and grain boundary migration followed by grain growth[172]. Micro-tensile experiments have proven very useful for nano-crystalline specimen, which are difficult to synthesize in bulk. Grain boundary-mediated processes have been directly captured in TEM under stress[169]. Experiments have been carried out for a constant grain size and changing pillar diameters and vice versa to determine which of the effect is playing a stronger role[9]. Since in small-scale specimens it is difficult to decouple the extrinsic from the intrinsic effects, Greer *et al.* have re-plotted the available data by normalizing the specimen dimension (D) with that of the internal length scale (d), demonstrating a 'smaller is weaker'

Figure 14. *a*, Sketch of a free-standing nc–Al film on a deformable Cu grid with the enlarged view showing the bright field and dark field micrographs of a 100 μm crack in a 380 nm thick nc–Al film prior to deformation. The last part of the enlarged view indicates that the initial grain size and microstructure is preserved except for the one grain located at the very tip of the crack; *b*, Dark field micrographs taken with the same *g* vector during an *in-situ* TEM tensile experiment on a 180 nm thick Al film. M and N are fixed points across the crack. Grain A is stretched as the crack opens; *c*, Grain length is plotted against crack opening[169].

trend below a critical D/d ratio unlike the case of single crystal specimen[9]. These results are even more interesting because this reversal is observed for grain sizes which otherwise fall in the traditional Hall–Petch regime for bulk specimen and is explained by the overlap of free surface effects with that of internal interfaces. Increase in the volume fraction of surface grains brings about a reduction in strength due to constraint free accommodation in the softer outer core. Incorporating image stresses experienced by dislocations near the free surface and the reduction in Taylor factor of surface grains in the calculations is able to explain the observed trends well. Recent experiments on wire drawn UFG Ni have shown a synergistic influence of reducing both the internal and external size scales in approaching theoretical strength of the material[173]. The authors carried out tensile tests on Ni micro-wires, whose microstructures were similar to heavily cold worked metals and found higher tensile strengths (3.3 GPa) in comparison to nano-wires (2.5 GPa). This was accompanied by a distinct change in fracture morphology from conventional void nucleation and growth-controlled necking to a chisel shape with limited cavitation and profuse shear banding. A detailed explanation for the mechanism driving such enhanced strengthening in a material full of dislocation defects is still lacking. Their work explores the middle domain between large polycrystals which do not exhibit any extrinsic size effect and nano-crystals where pronounced size effect is seen. Such fine scale structural variations also become impor-

tant when small volumes of materials are being tested, such as below the sharp tip of a nano-indenter, which also bring an additional variable in terms of strain gradient-based indentation size effect.

There have been much fewer reports on nano-laminate composites, notably on Cu/Nb-and fcc/bcc materials combination grown by sputtering[174,175] and TiAl, an inter-metallic with an intrinsic lamellar microstructure[161]. The laminate layer spacing controls the strengthening in these materials, irrespective of specimen size. Thin film specimens deposited by sputtering processes generally possess grain sizes of the order of film thickness. Both free standing metallic films and film–substrate combinations have been examined for their mechanical response to thermal and mechanical strains with varying film thickness[176–178]. A significant increase in flow stress was recorded with decreasing film thickness in both Cu and Al polycrystalline specimen[161]. Again a difference was found between polycrystalline films and epitaxially grown ones with the size effect more pronounced for polycrystalline ones. The Nix-Freund model of threading dislocations constrained by the film–substrate interface, depositing interfacial dislocations during their advancement through the film, has been used to explain these effects. Such a dislocation channelling mechanism is unable to quantify the behaviour of polycrystalline films, though the results agree well with those of epitaxial films. Free standing Al thin films of 100 to 400 nm thickness, obtained by Si micro-fabrication techniques, were tested in tension at room

temperature by Gianola and colleagues (Figure 14)[179–181]. Their results from *in-situ* TEM and surface relief measurements in AFM showed an unstable nanostructure in these films under stress with the nano-crystalline grains collapsing accompanied by grain boundary migration before any dislocation activity occurred at the crack tips. This preferential grain growth at crack tips is suggested as a toughening mechanism, enhancing the tensile ductility of these thin films. The large volume fraction of grain boundaries in films with less than 100 nm grains are attributed as the driving force for grain growth. On the other hand, a systematic increase in the impurity content stabilized the microstructure, preventing grain boundary migration, bringing about high strength and brittle behaviour in these films. The authors suggest this as a potential processing control that can be introduced to tailor the mechanical behaviour of nano-crystalline thin films in structural applications[181].

The combined effects of both the intrinsic and extrinsic length scales are not yet well understood with various other factors like specimen purity, experimental conditions, artifacts, geometry and synthesis or fabrication methods affecting the observed trends. Gianola and Eberl[19] have highlighted the effect of difference in experimental boundary conditions on the observed trends and the need to de-convolute experimental artifacts from real size effects as a material property. They compared results obtained from specimens tested in tension and pillar compression, both fabricated using FIB, to different aspect ratios. The strengthening seen in specimens of aspect ratios above 2 : 1, as in the tensile specimens, was much less prominent compared to that obtained using lower aspect ratios of pillars. A careful consideration to these has to be given when comparing results from different research groups. Also most of these experiments have dealt with hardness and flow stress changes with size, while very little information is available on the influence of reduced dimensions on other mechanical properties like fracture toughness, creep, ductility and fatigue life. These domains are yet to be studied in detail.

Summary and current outlook

Small scale testing has taken off in a big way in the past two decades or so due to the demands of continuously decreasing device sizes. Rapid progress has been made in instrumentation, enabling measurement of loads as low as few pico-newtons and resolve sub-nanometric displacements in combination with various direct *in-situ* viewing methods. Selected examples given in this review highlight both the capabilities achieved today in small scale testing and the need to do more with regards to going truly 'sub-nano'. There are open questions to be answered and domains where information is yet to be populated, which signals an opportunity to get into research in this field in a big way. It also calls for collaborative research,

sharing of information between various groups, and establishing standard practices across the globe. With components continuing to scale down in size, focus will shift to property interactions and influence of mechanical loads on functional properties of materials. Maintaining integrity and long lasting features at such small length scales holds the key to engineering materials in the new century. The Indian Institute of Science, Bangalore, and the Defence Metallurgical Research Laboratory, Hyderabad, have established various state-of-the-art facilities for mechanical testing of materials all the way down to the nano-scale which will initiate cutting edge research in small scale materials and systems. Equipments such as dual-beam FIB, e-beam lithography, nano-indenters with high temperature and scratch facilities, atomic force microscopes, nano-tribometers, micro-tensile testers, wafer curvature measurement machines, *in-situ* indentation and wear set-up inside the TEM, micro-Raman spectroscopic techniques to name a few, have been established. Two dedicated centers, viz. Advanced Facility for Microscopy and Microanalysis and Centre for Nano Science and Engineering have been setup in IISc for probing nano-scale systems and fuelling research at the small scale. Using the above facilities, miniaturized specimens have been fabricated out of TBCs, MEMS, thin films and carbon nano-tubes and their mechanical properties evaluated, the results of some of which are presented in this paper.

1. Bazant, Z. P., Size effect. *Int. J. Solid Struct.*, 2000, **37**, 69–80.
2. Griffith, A. A., The phenomena of rupture and flow of solids, JSTOR. *Philos. Trans. R. Soc. London A*, 1921, **221**, 163–198.
3. Hall, E., The deformation and ageing of mild steel 3. Discussion of results. *Proc. Phys. Soc. London B*, 1951, **64**, 747–753.
4. Petch, N. J., The cleavage strength of polycrystals. *J. Iron Steel Inst.*, 1953, **174**, 25–28.
5. Brenner, S. S., Tensile strength of whiskers. *J. Appl. Phys.*, 1956, **27**, 1484–1491.
6. Mechanical and Physical Properties of Whiskers. *CRC Handbook of Chemistry and Physics*, CRC Press, Cleaveland, 1974–75, 55th edn.
7. Shan, Z. W., Mishra, R. K., Syed Asif, S. A., Warren, O. L. and Minor, A. M., Mechanical annealing and source limited deformation in submicrometer diameter Ni crystals. *Nat. Mat.*, 2007, **7**, 115–119.
8. Chokshi, A. H., Rosen, A., Karch, J. and Gleiter, H., On the validity of the Hall–Petch relationship in nanocrystalline materials. *Scr. Metall.*, 1989, **23**, 1679–1684.
9. Greer, J., Exploring deformation mechanisms in nanostructured materials. *J. Met.*, 2012, **64**, 1241–1252.
10. Koch, C. C. and Narayan, J., The inverse Hall–Petch effect – fact or artifact? *Mater. Res. Soc. Symp. Proc.*, 2001, **634**, B5.1.1.
11. Freund, L. B. and Suresh, S., *Thin Film Materials: Stress, Defect Formation and Surface Evolution*, Cambridge University Press, 2009, 1st edn.
12. Srikar, V. T. and Spearing, F. M., A critical review of microscale mechanical testing methods used in the design of microelectromechanical systems. *Exp. Mech.*, 2003, **43**, 238–247.
13. Masuzawa, T., State of the art of micromachining. *Ann. CRIP*, 2000, **49**, 473.
14. Landolt, T., Chauvy, P. F. and Zinger, O., Electrochemical micromachining, polishing and surface structuring of metals: fundamental aspects and new developments. *Electrochem. Acta*, 2003, **48**, 3185–3201.

15. Yi, T. and Kim, C. J., Measurement of mechanical properties for MEMS materials. *Meas. Sc. Technol.*, 1999, **10**, 706–716.

16. Kamat, S. V., Experimental techniques for the measurement of mechanical properties of materials used in MEMS. *Def. Soc. J.*, 2009, **59**, 605–615.

17. Knauss, W. G., Chasiotis, I. and Huang, Y., Mechanical measurements at the micron and nanometer scales. *Mech. Mater.*, 2003, **35**, 217–231.

18. Fahlbusch, St, Nanomanipulations in a scanning electron microscope. *J. Mater. Proc. Technol.*, 2005, **167**, 371–382.

19. Gianola, D. S. and Eberl, C., The micro and nanoscale tensile testing of materials. *J. Metals*, 2009, **61**, 24–35.

20. Sharpe, W. N., Bagdahn, J., Jackson, K. and Coles, G., Tensile testing of MEMS materials-recent progress. *J. Mater. Soc.*, 2003, **38**, 4075–4079.

21. Prorok, B. C., *Encyclopedia of Nanoscience and Nanotech*, American Scientific Publishing, Valencia, 2004, vol. 5.

22. Connolley, T., A review of deformation and fatigue of metals at small size scales. *Fatigue Fract. Eng. Mater. Struc.*, 2005, **28**, 1119–1152.

23. Hemker, K. J. and Sharpe Jr, W. N., Microscale characterization of mechanical properties. *Annu. Rev. Mater. Res.*, 2007, **37**, 93–126.

24. Rich, D. B. and Christenson, J. C., Deep reactive ion etching process and microelectromechanical devices formed thereby. Delphi Technologies, Inc., 2001, Patent US7077007 B2.

25. Love, J. C., Estroff, L. A., Kriebel, J. K., Nuzzo, R. G. and Whitesides G. M., Self-assembled monolayers of thiolates on metals as a form of nanotechnology. *Chem. Rev.*, 2005, **105**, 1103–1169.

26. LaVan, D. A. and Sharpe Jr, W. N., Tensile testing of microsamples. *Expt. Mech.*, 1999, **39**, 210–216.

27. Lee, H. J., Choi, H. S., Han, C. S., Lee, N. K., Lee, G. A. and Choi, T. H., A precision alignment method of micro tensile testing specimen using mechanical gripper. *J. Mater. Proc. Technol.*, 2007, **241**, 187–188.

28. Wang, Y. M., Wang, K., Pan, D., Lu, K., Hemker, K. J. and Ma, E., Microsample tensile sample testing of nanocrystalline copper. *Scr. Mater.*, 2003, **48**, 1581–1586.

29. Järvelä, P. K., Method of measuring the strain of fibers in tension with the scanning electron microscope. *Fiber Sci. Technol.*, 1984, **20**, 83–90.

30. Chasiotis, I. and Knauss, W. G., A new microtensile tester for the study of MEMS materials with the aid of atomic force microscopy. *Expt. Mech.*, 2002, **42**, 51–57.

31. Hemker, K. J., Mendis, B. G. and Eberl, C., Characterizing the microstructure and mechanical behaviour of a two phase NiCo-CrAlY bond coat for thermal barrier systems. *Mater. Sci. Eng. A*, 2008, **483–484**, 727–730.

32. Orso, S., Wegst, U. G. K., Eberl, C. and Arzt, E., Micrometer scale tensile testing of biological attachment devices. *Adv. Mater.*, 2006, **18**, 874–877.

33. Pan, D., Chen, M. W., Wright, P. K. and Hemker, K. J., Evolution of a diffusion aluminide bond coat for thermal barrier coatings during thermal cycle. *Acta Mater.*, 2003, **51**, 2205–2217.

34. Louthan Jr, M. R., In *Tensile Testing of Metals and Alloys* (ed. Bacon, P.), Tensile Testing, ASM International, Ohio, 1993, p. 61.

35. ASTM Standard Test Methods for Tension Testing of Metallic Materials, ASTM E8/E8M-11, ASTM International, PA.

36. Nemeth, N. N., Evans, L. J., Jadaan, O. M., Sharpe, W. N., Beheim, G. M. and Trapp, M. A., Fabrication and probabilistic fracture strength prediction of high aspect ratio single crystal silicon carbide microspecimens with stress concentration. *Thin Solid Films*, 2007, **515**, 3283–3290.

37. El Zohairy, A. A., de Gee, A. J., de Jager, N., van Ruijven, L. J. and Feilzer, A. J., The influence of specimen attachment and dimension on microtensile strength. *J. Dent. Res.*, 2004, **83**, 420–424.

38. Meira, J. B. C., Ballester, R. Y., Lima, R. G., de Souza, R. M. and Driemeier, L., Geometrical aspects on bi-material microtensile tests. *J. Braz. Soc. Mech. Sci. Eng.*, 2005, **27**, 310–313.

39. Schwaiger, R., Fatigue behaviour of sub-micron silver and copper films, Ph D thesis, Max-Planck-Institut fur Metallforschung, Stuttgart, 2001.

40. Denis, Y. W. Y., Microtensile testing of free-standing and supported metallic thin film, Ph D thesis, Harvard University, Cambridge, Massachusetts, 2003.

41. Sharpe Jr, W. N., Turner, K. T. and Edwards, R. L., Tensile testing of polysilicon. *Expt. Mech.*, 1999, **39**, 162–170.

42. Jackson, K. M., Fracture strength, elastic modulus and Poisson's ratio of polycrystalline 3C thin film silicon carbide found by microsample tensile testing. *Sens. Actuat. A*, 2005, **125**, 34–40.

43. Sharpe Jr, W. N., Beheim, G., Nemeth, N. N., Evans, L. and Jadaan, O., Strength of single crystal silicon-carbide microspecimens at room and high temperature. In Proceedings of SEM Annual Conference and Exposition on Experimental and Applied Mechanics, 2005, pp. 1095–1101.

44. Alam, M. Z., Kamat, S. V., Jayaram, V. and Das, D. K., Tensile behaviour of a free-standing Pt-aluminide (PtAl) bondcoat. *Acta Mater.*, 2013, **61**, 1093–1105.

45. Eberl, C., Gianola, D. S., Wang, X., He, M. Y., Evans, A. G. and Hemker, K. J., A method for in situ measurement of the elastic behaviour of a columnar thermal barrier coating. *Acta Mater.*, 2011, **59**, 3612–3620.

46. Schuh, C. A., Nanoindentation studies of materials. *Mater. Today*, 2006, **9**, 32–40.

47. Fischer-Cripps, A. C., *Nanoindentation*, Springer, 2004, Second edition.

48. Uchic, M. D., Shade, P. A. and Dimiduk, D. M., Plasticity of micrometer-scale single crystals in compression. *Annu. Rev. Mater. Res.*, 2009, **39**, 361–386.

49. Fei, H., Abraham, A., Chawla, N. K. and Jiang, H., Evaluation of Micro-Pillar compression tests for accurate determination of elastic–plastic constitutive relations. *J. Appl. Mech.*, 2012, **79**, 061011-1–061011-9.

50. Kiener, D., Guruprasad, P. J., Keralavarma, S. M., Dehm, G. and Benzerga, A. A., Work-hardening in micropillar compression: *In situ* experiments and modeling. *Acta Mater.*, 2011, **59**, 3825–3840.

51. Timoshenko, S. P. and Goodier, J. N., *Theory of Elasticity*, Mc-Graw Hill Book Company, 1970, 3rd edn.

52. Kraft, O., Schwaiger, R. and Nix, W. D., Measurement of mechanical properties in small dimensions by microbeam deflection. *Mater. Res. Soc. Symp. Proc.*, 1998, **518**, 39–44.

53. Stoney, G. G., The tension of metallic films deposited by electrolysis. *Proc. R. Soc. London A*, 1909, **82**, 171–175.

54. Vlassak, J. J. and Nix, W. D., A new bulge test technique for the determination of Young's modulus and Poisson's ratio of thin films. *J. Mater. Res.*, 1992, **7**, 3242–3249.

55. Eskner, M. and Sandstrom, R., Measurement of the ductile-to-brittle transition temperature in a nickel aluminide coating by a miniaturised disc bending test technique. *Surf. Coat Technol.*, 2003, **165**, 71–80.

56. Cacchione, F., Masi, B. D., Corigliano, A. and Ferrera, M., Material characterization at the micro scale through on-chip tests, ICF11, Torino, 2005, pp. 20–25.

57. Corigliano, A., Cacchione, F., Masi, B. D. and Riva, C., On chip electrostatically actuated bending tests for the mechanical characterization of polysilicon at the micro scale. *Mechanica*, 2005, **40**, 485–503.

58. Haque, M. A. and Saif, M. T. A., Uniaxial tensile and bending experiments on nanoscale metal films. In Proceedings of SEM Annual Conference and Exposition on Experimental and Applied Mechanics, 2002.

59. Eberl, C., Fatigue of Al thin films at ultra high frequencies, Ph D thesis, Max Planck Institute for Metallforschung, Stuttgart, 2005.

60. Binning, G. and Rohrer, H., Scanning tunneling microscopy. *Helv. Phys. Acta*, 1982, **55**, 726–735.

61. Eigler, D. M. and Shweizer, D. K., Positioning single atoms with a scanning tunneling microscope. *Nature*, 1990, **344**, 524–526.

62. Hatamura, Y. *et al.*, Direct coupling system between nanometer world and human world. *Proc. IEEE Conf. MEMS*, 1990, 203–208.

63. Kasaya, T., Miyazaki, H., Saito, S. and Sato, T., Micro object handling under SEM by vision-based automatic control. *Proc. SPIE Int. Symp. Intell. Syst. Adv. Manuf.*, 1998, **135**, 181–192.

64. Fatikow, S., Seyfried, J., Fahlbusch, S., Buerkle, A. and Schmoeckel, F., A flexible micro-robot based micro-assembly station. *J. Intell. Rob. Syst.*, 2000, **27**, 135–169.

65. Lim, C. T., Zhou, E. H., Li, A., Vedula, S. R. K. and Fu, H. X., Experimental techniques for single cell and single molecule biomechanics. *Mater. Sci. Eng. C. Biomimet. Supramol. Syst.*, 2006, **26**, 1278–1288.

66. Tamarin, Y., Choosing optimum coatings for modern aircraft engine turbine blades, protective coatings for turbine blades, Ohio ASM International, 2002, p. 13.

67. Bose, S., High-temperature corrosion. In *High Temperature Coatings*, Butterworth-Heinemann Publications, Oxford, 2007, p. 53.

68. Padture, N. P., Source; www.matsceng.ohio-state.edu

69. Sourmail, T., Coatings for turbine blades (Source: http://www.msm.cam.ac.uk/phase-trans/2003/Superalloys/coatings/index.html).

70. Evans, A. G., Mumm, D. R. and Hutchinson, J. W., Mechanisms controlling the durability of thermal barrier coatings. *Progr. Mater. Sci.*, 2001, **46**, 505–553.

71. Chen, J. H. and Little, J. A., Degradation of the platinum aluminide coating on CMSX4 at 1100°C. *Surf. Coat. Technol.*, 1997, **92**, 69–77.

72. Das, D. K., Microstructure and high temperature oxidation behaviour of Pt-modified aluminide bond coats on Ni-base superalloys. *Progr. Mat. Sci.*, 2013, **58**, 151–182.

73. Alam, M. Z., Hazari, N., Varma, V. K. and Das, D. K., Effect of cyclic oxidation exposure on tensile properties of a Pt-aluminide bond coated Ni-base superalloy. *Metall. Mater. Trans. A*, 2011, **42**, 4064–4074.

74. Pugacheva, N. B. and Kositsyn, S. V., Special features of fracture of nickel alloys with a diffusion aluminide coat in tensile and low cycle fatigue tests. *Metal. Sci. Heat Treatment*, 1999, **41**, 117–120.

75. Hancock, P., Chien, H. H., Nicholls, J. R. and Stephenson, D. J., *In-situ* measurements of the mechanical properties of aluminide coatings. *Surf. Coats Technol.*, 1990, **43–44**, 359–370.

76. Antelo, M. A., Johnson, P. K., Ostolaza, K. M. and Bressers, J., Analysis of the fracture behaviour of an aluminide coating on a single-crystal superalloy under tensile conditions. *Mat. Sci. Eng.*, 1998, **247**, 40–50.

77. Totemeier, T. C., Gale, W. F. and King, J. E., Fracture behaviour of an aluminide coating on a single crystal nickel base superalloy. *Mat. Sci. Eng.*, 1993, **169**, 19–26.

78. Zhang, M. and Heuer, A. H., Spatially varying microhardness in a platinum-modified nickel aluminide bond coat in a thermal barrier coating system. *Scr. Mat.*, 2006, **54**, 1265–1269.

79. Dryepondt, S. and Pint, B. A., Determination of the ductile to brittle temperature transition of aluminide coatings and its influence on the mechanical behaviour of coated specimens. *Surf. Coat Technol.*, 2010, **205**, 1195–1199.

80. Alam, M. Z., Srivathsa, B., Hazari, N., Kamat, S. V., Jayaram, V. and Das, D. K., Mechanism of failure in a free-standing Pt-aluminide bond coat during tensile testing at room temperature. *Mater. Sci. Eng. A*, 2010, **527**, 842–848.

81. Zhao, M., Chen, X., Yan, J. and Karlsson, A. M., Determination of uniaxial residual stress and mechanical properties by instrumented indentation. *Acta Mater.*, 2006, **5**4, 2823–2832.

82. Potnis, P., Holtzinger, J., Das, D., Jayaram, V. and Biswas, S. K., Study of fracture behaviour of bond coats on nickel superalloy by three-point bending of microbeams. *Surf. Coat Technol.*, 2009, **204**, 586–592.

83. Jaya, B. N., Jayaram, V. and Biswas, S. K., A new method for fracture toughness determination of graded (Pt,Ni)Al bond coats by microbeam bend tests. *Philos. Mag.*, 2012, **92**, 3326–3345.

84. Webler, R., Krottenthaler, M., Neumeier, S., Durst, K. and Goken, M., Local fracture properties and residual stress measurements on NiAl bond coats by micro-cantilever and FIB-based bar milling tests. *Superalloys*, 2012, 93–102.

85. Zhou, Y. C., Hashida, T. and Jian, C. Y., Determination of interface fracture toughness in thermal barrier coating system by blister tests. *Trans. ASME*, 2003, **125**, 176–182.

86. Arai, M., Okajima, Y. and Kishimoto, K., Mixed-mode interfacial fracture toughness for thermal barrier coating. *Eng. Frac. Mech.*, 2007, **74**, 2055–2069.

87. Eberl, C., Gianola, D. S. and Hemker, K. J., Mechanical characterization of coatings using microbeam bending and digital image correlation techniques. *Exp. Mech.*, 2008, **50**, 85–97.

88. Eberl, C., Gianola, D. S., Wang, X., He, M. Y., Evans, A. G. and Hemker, K. J., A method for *in situ* measurement of the elastic behaviour of a columnar thermal barrier coating. *Acta Mater.*, 2011, **59**, 3612–3620.

89. Eberl. C., Wang, X., Gianola, D. S., Nguyen, T. D., He, M. Y., Evans, A. G. and Hemker, K. J., *In situ* measurement of the toughness of the interface between a thermal barrier coating and a Ni alloy. *J. Am. Ceram. Soc.*, 2011, **94**, S120–S127.

90. Thery, P. Y., Poulain, M., Dupeux, M. and Braccini, M., Adhesion energy of a YPSZ EB-PVD layer in two thermal barrier coating systems. *Surf. Coats Technol.*, 2007, **202**, 648–652.

91. Liu, D., Qingfen, L., Yulong, L. and Aliabadi, M. H., The measurement of mechanical properties of thermal barrier coatings by micro-cantilever tests. *Key Eng. Mat.*, 2013, **525–526**, 13–16.

92. Alam, M. Z., Srivathsa, B., Kamat, S. V., Jayaram, V. and Das, D. K., Microtensile testing of a free-standing Pt-aluminide bond coat. *Mat. Design*, 201, **32**, 1242–1252.

93. Alam, M. Z., Tensile behaviour of stand-alone Pt-aluminide (PtAl) bond coats, Ph D thesis, Indian Institute of Science (IISc), Bangalore, India, 2012.

94. Schweitz, J. A., Mechanical characterization of thin films by micromechanical techniques. *MRS Bull.*, 1992, **17**, 34–45.

95. Arzt. E., Size effects in materials due to microstructural and dimensional constraints: A comparative review. *Acta Mater.*, 1998, **46**, 5611–5626.

96. Ding, J. N., Meng, Y. G. and Wen, S. Z., Specimen size effect on mechanical properties of polysilicon microcantilever beams measured by deflection using a nanoindenter. *Mat. Sci. Eng. B*, 2001, **83**, 42–47.

97. Sharpe, W. N., Yuan, B., Vaidyanathan, R. and Edwards, R. L., New test structures and techniques for measurement of mechanical properties of MEMS materials. *Proc. SPIE*, 1996, **2880**, 78–91.

98. Kapels, H., Aigner, R. and Binder, J., Fracture strength and fatigue of poly-Si determined by a novel thermal actuator. *IEEE Trans. Electron Dev.*, 2000, **4**7, 1522–1528.

99. Tsuchiya, T., Tabata, O., Sakata, J. and Taga, Y., Specimen size effect on tensile strength of surface-micromachined polycrystalline silicon thin films. *J. MEMS*, 1998, **7**, 106–113.

100. Ando, T., Li, X., Nakao, S., Kasai, T., Shikida, M. and Sato, K., Effect of crystal orientation on fracture strength and fracture toughness of single crystal silicon. *IEEE Int. Conf. MEMS*, 2004, 177–180.

101. Son II, D., Kim, J. J. and Kwon, D., Fracture behaviour of single- and polycrystalline silicon films for MEMS applications. *Key Eng. Mat.*, 2005, **297–300**, 551–556.

102. Tsuchiya, T., Tensile testing of silicon thin films. *Fatigue Frac. Eng. Mat. Struc.*, 2005, **28**, 665–674.

103. Kahn, H., Fracture toughness of polysilicon MEMS devices. *Sens. Actuat. A*, 2000, **82**, 274–280.

104. Ando, T., Li, X., Nakao, S., Kasai, T., Tanaka, H., Shikda, M. and Sato, K., Fracture toughness measurement of thin-film silicon. *Fatigue Frac. Eng. Mat. Struc.*, 2005, **28**, 687–694.

105. Bagdahn, J., Schischka, J., Petzola, M. and Sharpe Jr, W. N., Fracture toughness and fatigue investigations of polycrystalline silicon. *Proc. SPIE*, 2001, **4558**, 159–168.

106. Ballarini, R., Mullen, R. L., Yin, Y., Kahn, H., Stemmer, S. and Heuer, A. H., The fracture toughness of poly-Si micro devices – A first report. *J. Mat. Res.*, 1997, **12**, 915–922.

107. Boroch, R., Wiaranowski, J., Mueller-Fiedler, R., Ebert, M. and Bagdahn, J., Characterization of strength properties of thin polycrystalline silicon films for MEMS applications. *Fatigue Frac. Eng. Mat. Struc.*, 2007, **30**, 2–12.

108. Namazu, T., Isono, Y. and Tanaka, T., Evaluation of size effect on mechanical properties of single crystal silicon by nanoscale bending test using AFM. *J. Microelectromech. Syst.*, 2000, **9**, 450–459.

109. Fitzgerald, A. M., Dauskardt, R. H. and Kenny, T. W., Fracture toughness and crack growth phenomena of plasma-etched single crystal silicon. *Sens. Actuat. A*, 2000, **83**, 194–199.

110. Ebrahimi, F. and Kalwani, L., Fracture anisotropy in silicon single crystal. *Mat. Sci. Eng. A*, 1999, **268**, 116–126.

111. Li, X., Kasai, T., Nakao, S., Ando, T. and Shikida, M., Anisotropy in fracture of single crystal silicon film characterized under uniaxial tensile condition. *Sens. Actuat. A*, 2005, **117**, 143–150.

112. Alsem, D. H., Pierron, O. N., Stach, E. A., Muhlstein, C. L. and Ritchie, R. O., Mechanisms for fatigue of micron-scale silicon structural films. *Adv. Eng. Mat.*, 2007, **9**, 15–30.

113. Thouless, M. D. and Cook, R. F., Stress-corrosion cracking in silicon. *Appl. Phys. Lett.*, 1990, **56**, 1962–1964.

114. Muhlstein, C. L., Brown, S. B. and Ritchie, R. O., High-cycle fatigue of polycrystalline silicon thin films in laboratory air. *MRS Symp. Proc.*, 2000, **657**, EE5.8.1–EE5.8.6.

115. Kahn, H., Ballarini, R., Mullen, R. L. and Heuer, A. H., Electrostatically actuated failure of microfabricated polysilicon fracture mechanics specimens. *Proc. R. Soc. London A*, 1999, **455**, 3807–3823.

116. Sharpe Jr, W. N. and Turner, K. T., Fatigue testing of materials used in microelectromechanical systems. In *7th International Fatigue Congress*, 1999, pp. 1837–1844.

117. Muhlstein, C. L., Brown, S. B. and Ritchie, R. O., High cycle fatigue and durability of polycrystalline Si thin films in ambient air. *Sens. Actuat. A*, 2001, **94**, 177–188.

118. Alsem, D. H. *et al.*, Fatigue failure in thin-film polycrystalline silicon is due to subcritical cracking within the oxide layer. *Appl. Phys. Lett.*, 2005, **86**, 041914-1–041914-3.

119. Kahn, H., Ballarini, R. and Heuer, A. H., Effects of varying mean stress and stress amplitude on the fatigue of polysilicon. *Mat. Res. Soc. Symp. Proc.*, 2004, U.4.7.1–U.4.7.9.

120. Ritchie, R. O., Kruzic, J. J., Muhlstein, C. L., Nalla, R. K. and Stach, E. A., Characteristic dimensions and the micro-mechanisms of fracture and fatigue in 'nano' and 'bio' materials. *Int. J. Fract.*, 2004, **128**, 1–15.

121. Muhlstein, C. L., Stach, E. A. and Richie, R. O., Mechanism of fatigue in micron-scale films of polycrystalline silicon for microelectromechanical systems. *Appl. Phys. Lett.*, 2002, **80**, 1532–1535.

122. Muhlstein, C. L., Stach, E. A. and Richie, R. O., A reaction-layer mechanism for the delayed failure of micron-scale polycrystalline silicon structural films subjected to high-cycle fatigue loading. *Acta Mat.*, 2002, **50**, 3579–3595.

123. Allameh, S. M., Shrotriya, P., Butterwick, A., Brown, S. B. and Soboyejo, W. O., Surface topography: evolution and fatigue fracture in polysilicon MEMS structures. *J. MEMS*, 2003, **12**, 313–324.

124. Muhlstein, C. and Ritchie, R. O., High-cycle fatigue of micron-scale polycrystalline silicon films: fracture mechanics analyses of the role of the silica/ silicon interface. *Int. J. Fract.*, 2003, **119/120**, 449–474.

125. Gerberich, W. W., Mook, W. M. and Perry, C. R., Superhard silicon nanospheres. *J. Mech. Phys. Solids*, 2003, **51**, 979–992.

126. Deneen, J., Mook, W. M., Minor, A., Gerberich, W. W. and Carter, C. B., *In situ* deformation of silicon nanospheres. *J. Mater. Sci.*, 2006, **41**, 4477–4483.

127. Lockwood, A. J. and Inkson, B. J., *In situ* TEM nanoindentation and deformation of Si-nanoparticle clusters. *J. Phys. D: Appl. Phys.*, 2009, **42**, 035410-1–035410-5.

128. Zhang, N. *et al.*, Deformation mechanisms in Si nanoparticles. *J. Appl. Phys.*, 2011, **109**, 063534-1–063534-6.

129. Ostlund, F. *et al.*, Brittle-to-ductile transition in uniaxial compression of silicon pillars at room temperature. *Adv. Funct. Mat.*, 2009, **19**, 2439–2444.

130. Meyers, M. A., Chen, P. Y., Lin, A. Y. and Seki, Y., Biological materials: Structure and mechanical properties. *Progr. Mat. Sci.*, 2008, **53**, 1–206.

131. Suresh, S. *et al.*, Connections between single-cell biomechanics and human disease states: gastrointestinal cancer and malaria. *Acta Biomater.*, 2005, **1**, 15–30.

132. Suresh, S., Biomechanics and biophysics of cancer cells. *Acta Biomater.*, 2007, **3**, 413–438.

133. Barthelat, F., Rim, J. E. and Espinosa, H. D., A review on the structure and mechanical properties of mollusk shells – perspectives on synthetic biomimetic materials. In *Applied Scanning Probe Methods – Biomimetics and Industrial Applications*, Springer-Verlag, Berlin-Heidelberg, 2009, chapter 19, pp. 17–44.

134. Bruet, B. J. F. *et al.*, Nanoscale morphology and indentation of individual nacre tablets from the gastropod mollusk: *Trochus niloticus*. *J. Mater. Res.*, 2005, **20**, 2400–2419.

135. Barthelat, F., Li, C. M., Comi, C. and Espinosa, H. D., Mechanical properties of nacre constituents and their impact on mechanical performance. *J. Mat. Res.*, 2006, **21**, 1977–1986.

136. Smith, B. L. *et al.*, Molecular mechanistic origin of the toughness of natural adhesives, fibres and composites. *Nature (London)*, 1999, **399**, 761–763.

137. Oyen, M. L., Nanoindentation of biological and biomimetic materials. *Exp. Tech.*, 2013, **37**, 73–87.

138. Jackson, A. P., Vincent, J. F. V. and Turner, R. M., The mechanical design of nacre. *Proc. R. Soc. London*, 1988, **234**, 1277, 415–440.

139. Sarikaya, M., Gunnison, K. E., Yasrebi, M. and Aksay, I. A., *Mat. Res. Soc. Symp. Proc.*, 1990, **174**, 109–116.

140. Menig, R., Meyers, M. H., Meyers, M. A. and Vecchio, K. S., Quasi-static and dynamic mechanical response of *Haliotis rufescens* (abalone) shells. *Acta Mater.*, 2000, **48**, 2383–2398.

141. Wang, R. Z., Suo, Z., Evans, A. G., Yao, N. and Aksay, I. A., Deformation mechanisms in nacre. *J. Mater. Res.*, 2001, **16**, 2485–2493.

142. Barthelat, F. and Espinosa, H. D., An experimental investigation of deformation and fracture of nacre-mother of pearl. *Exp. Mech.*, 2007, **47**, 311–324.

143. Sarikaya, M. and Aksay, I. A. (eds), *Biomimetics, Design and Processing of Materials*, Woodbury, NY, 1995.

144. Tang, Z., Kotov, N. A., Magonov, S. and Ozturk, B., Nanostructured artificial nacre. *Nat. Mat.*, 2003, **2**, 413–418.

145. Chen, L., Ballarini, R., Kahn, H. and Heuer, A. H., Bioinspired micro-composite structure. *J. Mater. Res.*, 2007, **22**, 124–131.

146. Verma, N., Mechanism and modeling of contact damage in ZrN–Zr and TiAlN–TiN multilayer hard coatings, Ph D thesis, Indian Institute of Science, Bangalore, 2012.

147. Raghavan, S. and Redwing, J. M., *In situ* stress measurements during the MOCVD growth of AlN buffer layers on (111)Si substrates. *J. Cryst. Growth*, 2004, **261**, 294–300.

148. Raghavan, S. and Redwing, J. M., Growth stresses and cracking in GaN films on (111)Si grown by metalorganic chemical-vapor deposition. I. AlN buffer layers. *J. Appl. Phys.*, 2005, **98**, 023514-1–023514-9.

149. Krost, A. *et al.*, *In situ* monitoring of the stress evolution in growing group-III-nitride layers. *J. Cryst. Growth*, 2005, **275**, 209–216.

150. Hearne, S. *et al.*, Stress evolution during metalorganic chemical vapor deposition of GaN. *Appl. Phys. Lett.*, 1999, **74**, 356–368.

151. Kim, M. H., Do, Y. G., Kang, H. C., Noh, D. Y. and Park, S. J., Effect of step-graded AlGaN interlayer on properties of GaN grown on Si(111) using ultrahigh vacuum chemical vapour deposition. *Appl. Phys. Lett.*, 2001, **79**, 2713–2715.

152. Li, W. and Ni, W. X., Residual strain in GaN epilayers grown on sapphire and (6H)SiC substrates. *Appl. Phys. Lett.*, 1996, **68**, 2705–2707.

153. Kozawa, T., Kachi, T., Kano, H., Nagase, H., Koide, N. and Manabe, K., Thermal stress in GaN epitaxial layers grown on sapphire substrates. *J. Appl. Phys.*, 1995, **77**, 4389–4392.

154. Vennéguès, P., Beaumont, B., Vaille, M. and Gibart, P., Microstructure of GaN epitaxial films at different stages of the growth process on sapphire (0001). *J. Cryst. Growth*, 1997, **173**, 249–259.

155. Raghavan, S., Weng, X., Dickey, E. and Redwing, J. M., Correlation of growth stress and structural evolution during metalorganic chemical vapor deposition of GaN on (111) Si. *Appl. Phys. Lett.*, 2006, **88**, 041904-1–041904-3.

156. Raghavan, S., Kinetic approach to dislocation bending in low-mobility films. *Phys. Rev. B*, 2011, **83**, 052102-1–052102-4.

157. Lee, S. R., Koleske, D. D., Corss, K. C., Floro, J. A. and Waldrip, K. E., *In-situ* measurements of the critical thickness for strain relaxation in AlGaN/GaN heterostructures. *Appl. Phys. Lett.*, 2004, **85**, 6164–6166.

158. Holec, D., Zhang, Y., Rao, D. V. S., Kappers, M. J., McAleese, C. and Humphreys, C. J., Equilibrium critical thickness for misfit dislocations in III-nitrides. *J. Appl. Phys.*, 2008, **104**, 123514-1–123514-7.

159. Holec, D., Critical thickness calculations for In$_x$Ga$_{1-x}$N/GaN systems, Ph D thesis, 2006.

160. Bazant, Z. P., Size effect on structural strength: a review. *Arch. Appl. Mech.*, 1999, **69**, 703–725.

161. Dehm, G., Motz, C., Scheu, C., Clemens, H., Mayrhofer, P. H. and Mitterer, C., Mechanical size effects in miniaturized and bulk materials. *Adv. Eng. Mat.*, 2006, **8**, 1033–1045.

162. Gerberich, W. W. *et al.*, Nanoprobing fracture length scales. *Int. J. Fract.*, 2006, **138**, 75–100.

163. Greer, J., Hosson, J. and De, Th. M., Plasticity in small-sized metallic systems: Intrinsic versus extrinsic size effect. *Progr. Mat. Sci.*, 2011, **56**, 654–724.

164. Brenner, S. S., Tensile strength of whiskers. *J. Appl. Phys.*, 1956, **27**, 1484–1491.

165. Kiener, D. and Minor, A. M., Source truncation and exhaustion: Insights from quantitative *in situ* TEM tensile testing. *Nanoletters*, 2011, **11**, 3816–3820.

166. Bei, H., Shim, S., Miller, M. K., Pharr, G. M. and George, E. P., Effects of focused ion beam milling on the nanomechanical behaviour of a molybdenum-alloy single crystal. *Appl. Phys. Lett.*, 2007, **91**, 111915-1–111915-3.

167. Shan, Z. W. *et al.*, Ultrahigh stress and strain in hierarchically structured hollow nanoparticles. *Nat. Mat.*, 2008, **7**, 947–952.

168. Mompiou, F., Legros, M., Sedlmayr, A., Gianola, D. S., Caillard, D. and Kraft, O., Source-based strengthening of sub-micrometer Al fibers. *Acta Mater.*, 2012, **60**, 977–983.

169. Legros, M., Gianola, D. S. and Motz, C., Quantitative *in-situ* mechanical testing in electron microscopes. *MRS Bull.*, 2010, **35**, 354–360.

170. Fleck, N. A., Muller, G. M., Ashby, M. F. and Hutchinson, J. W., Strain gradient plasticity: Theory and experiment. *Acta Metall. Mater.*, 1994, **42**, 475–487.

171. Ng, K. S. and Ngan, A. H. W., Effects of trapping dislocations within small crystals on their deformation behaviour. *Acta Mater.*, 2009, **57**, 4902–4910.

172. Carlton, C. E. and Ferreira, P. J., What is behind the inverse Hall–Petch effect in nanocrystalline materials? *Acta Mater.*, 2007, **55**, 3749–3756.

173. Warthi, N., Ghosh, P. and Chokshi, A. H., Approaching theoretical strengths by synergistic internal and external size refinement. *Scr. Mater.*, 2013, **68**, 225–228.

174. Thilly, L., Van Petegem, S., Renault, P. O., Lecouturier, F., Vidal, V., Schmitt, B. and Van Swygenhoven, H., A new criterion for elastoplastic transition in nanomaterials: Application to size and composite effects on Cu–Nb nanocomposite wires. *Acta Mater.*, 2009, **57**, 3157–3169.

175. Mara, N. A., Bhattacharyya, D., Dickerson, P., Hoagland, R. G. and Misra, A., Deformability of ultrahigh strength 5 nm Cu/Nb nanolayered composites. *Appl. Phys. Lett.*, 2008, **92**, 231901-1–231901-3.

176. Balk, T. J., Dehm, G. and Arzt, E., Parallel glide: unexpected dislocation motion parallel to the substrate in ultrathin copper films. *Acta Mater.*, 2003, **51**, 4471–4485.

177. Legros, M., Dehm, G., Keller, R. M., Arzt, E., Hemker, K. J. and Suresh, S., Dynamic observation of Al thin films plastically strained in a TEM. *Mater. Sci. Eng. A,* 2001, **309/310**, 463–467.

178. Kobrinsky, M. J., Dehm, G., Thompson, C. V. and Arzt, E., Effects of thickness on the characteristic length scale of dislocation plasticity in Ag thin films. *Acta Mater.*, 2001, **49**, 3597–3607.

179. Legros, M., Gianola, D. S. and Hemker, K. J., *In situ* TEM observations of fast grain boundary motion in stressed nanocrystalline aluminum films. *Acta Mater.*, 2008, **56**, 3380–3393.

180. Gianola, D. S., Eberl, C., Cheng, X. M. and Hemker, K. J., Stress-driven surface topography evolution in nanocrystalline Al thin films. *Adv. Mat.*, 2008, **20**, 303–308.

181. Gianola, D. S., Warner, D. H., Molinari, J. F. and Hemker, K. J., Increased strain rate sensitivity due to stress-coupled grain growth in nanocrystalline Al. *Scr. Mater.*, 2006, **55**, 649–652.

182. Bhowmick, S., Syed Asif, S. A., Warren, O. L., Jaya N. B., Jayaram, V. and Biswas, S. K., *In-situ* SEM study of microbeam bending of diffusion aluminide bond coats. *Microsc. Microanal.*, 2012, **18**, S2, 780–781.

183. Uchic, M. D., Dimiduk, D. M., Florando, J. N. and Nix, W. D., Sample dimension influences crystal strength and plasticity. *Science*, 2004, **305**, 986–989.

184. Rabe, R., Breguet, J. M., Schwaller, P., Stauss, S., Hauga, F. J., Patscheider, J. and Michler, J., Observation of fracture and plastic deformation during indentation and scratching inside the scanning electron microscope. *Thin Sol. Films*, 2004, **469–470**, 206–213.

185. Knauss, W. G., Chasiotis, I. and Huang, Y., Mechanical measurements at the micron and nanometer scales. *Mech. Mater.*, 2003, **35**, 217–231.

186. Bao, G. and Suresh, S., Cell and molecular mechanics of biological materials. *Nat. Mat.*, 2003, **2**, 715–725.

187. Weng, X., Raghavan, S., Acord, J. D., Jain, A., Dickey, E. C. and Redwing, J. M., Evolution of threading dislocations in MOCVD-grown GaN films on (111) Si substrates. *J. Cryst. Growth*, 2007, **300**, 217–222.